Calcium isotopic fractionation during adsorption onto and desorption from soil phyllosilicates (kaolinite, montmorillonite and muscovite)

Jean-Michel Brazier, Anne-Désirée Schmitt, Sophie Gangloff, Eric Pelt, François Chabaux, Emmanuel Tertre

▶ **To cite this version:**

Jean-Michel Brazier, Anne-Désirée Schmitt, Sophie Gangloff, Eric Pelt, François Chabaux, et al.. Calcium isotopic fractionation during adsorption onto and desorption from soil phyllosilicates (kaolinite, montmorillonite and muscovite). Geochimica et Cosmochimica Acta, 2019, 250, pp.324 - 347. 10.1016/j.gca.2019.02.017 . hal-03486799

HAL Id: hal-03486799
https://hal.science/hal-03486799

Submitted on 20 Dec 2021

HAL is a multi-disciplinary open access archive for the deposit and dissemination of scientific research documents, whether they are published or not. The documents may come from teaching and research institutions in France or abroad, or from public or private research centers.

L'archive ouverte pluridisciplinaire **HAL**, est destinée au dépôt et à la diffusion de documents scientifiques de niveau recherche, publiés ou non, émanant des établissements d'enseignement et de recherche français ou étrangers, des laboratoires publics ou privés.

Distributed under a Creative Commons Attribution - NonCommercial 4.0 International License

Version of Record: https://www.sciencedirect.com/science/article/pii/S0016703719300948
Manuscript_3011a32db4e6c54bd78c753b191f7886

Calcium isotopic fractionation during adsorption onto and desorption from soil phyllosilicates (kaolinite, montmorillonite and muscovite)

Jean-Michel Brazier[a], Anne-Désirée Schmitt[a], Sophie Gangloff[a], Eric Pelt[a], François Chabaux[a] and Emmanuel Tertre[b]

[a] Université de Strasbourg, CNRS, ENGEES, LHyGeS UMR 7517, 1 rue Blessig, F-67000 Strasbourg, France

[b] Universite de Poitiers/CNRS, UMR 7285 IC2MP, Equipe HydrASA, Bat. B8 rue Albert Turpain, TSA 51106-86073 Poitiers CEDEX 9, France

© 2019 published by Elsevier. This manuscript is made available under the CC BY NC user license
https://creativecommons.org/licenses/by-nc/4.0/

Abstract

Mineral soil constituents play an important role in the storage/release of nutrients due to their ability to adsorb and desorb cations. Phyllosilicate minerals are particularly reactive due to their small size and high specific surface area (up to ~800 $m^2.g^{-1}$). Previous work has highlighted the potential of Ca isotopes ($\delta^{44/40}Ca$) to identify secondary processes occurring within soils. Nevertheless, the mechanisms of isotopic fractionation (amplitude and nature) associated with Ca adsorption onto and desorption from different phyllosilicate minerals that are commonly found in soil remain poorly understood. This step is fundamental to improve our understanding of the Ca biogeochemical cycle at the water-soil-plant interface. Consequently, the study of the possible Ca isotopic fractionation during adsorption/desorption phenomena was approached experimentally using three "model" substrates representative of the phyllosilicate minerals frequently encountered within soils (KGa-2 kaolinite, Swy-2 montmorillonite and Tuftane muscovite). The experiments were carried out under abiotic conditions in "water-mineral" batch systems by precisely controlling the physico-chemical conditions: pH, solid/solution ratio, initial dissolved Ca concentration, particle size distribution, reaction time and other cations concentrations. Our results show no significant isotopic fractionation associated with Ca adsorption or desorption during KGa-2 and coarse size fraction of Tuftane muscovite (50-200 µm) experiments regardless of the physico-chemical parameters used. During Ca adsorption onto Swy-2 and fine size fraction of Tuftane muscovite (0.1-1 µm), light isotopes (e.g., ^{40}Ca) are preferentially adsorbed to the clay mineral, and a positive apparent isotopic fractionation between 0.10‰ and 0.28‰ is measured in the supernatant recovered after adsorption experiments. Kinetic and thermodynamic isotopic fractionation are observed during the Swy-2 experiments while only a thermodynamic fractionation took place during the Tuftane muscovite (0.1-1 µm)

experiments. The results obtained for the Ca desorption experiments performed with a chloride hexaamine cobalt solution suggest that Ca adsorption and the associated isotopic fractionation are fully reversible. Our results show that the Ca isotopic fractionation intensity during adsorption phenomena onto clay minerals is controlled by the layer charge and specific surface area of the considered phyllosilicate mineral, as well as the presence of an interlayer space open to cationic solute.

1. INTRODUCTION

Today, sustainable management of natural forest ecosystems is an important societal issue that requires a better understanding of nutrient dynamics at the water-soil-plant interface. Calcium (Ca) is a major macronutrient within soils, and it has an essential role in vegetation growth (Marschner, 1995; Berner and Berner, 1996; Taiz and Zeiger, 2010; Tipper et al., 2016). Consequently, its bioavailability raises questions, particularly in the case of nutrient depleted soils (e.g., acidic substratum and acidic rain).

At the global scale, Ca^{2+} is greatly affected by continental weathering through the dissolution of calcium silicates and carbonates via the consumption of atmospheric CO_2 (Walker et al., 1981; Meybeck, 1987; Fantle and Tipper, 2014; Schmitt, 2016). However, the current mean rivers' Ca isotopic signature arriving at the oceans ($\delta^{44/40}Ca$ = 0.86‰ relative to SRM915a) cannot be explained only by the contributions of continental weathering or vegetation uptake (Schmitt et al., 2003, Tipper et al., 2010; Fantle and Tipper, 2014). This implies that in addition to the fractionations induced by plant uptake (Schmitt et al., 2003; 2013; 2017; 2018; Holmden and Bélanger, 2010; Bagard et al., 2011; Cobert et al., 2011; Stille et al., 2012; Hindshaw at al., 2013) other continental processes, in particular occurring at the water-soil-plant interface, may potentially modify this signature. Several studies have suggested that adsorption/desorption processes involving mineral and/or organic compounds present in soils (clay minerals, Fe and Al oxy-hydroxides, and humic compounds) could also contribute to the isotopic signature of aqueous Ca arriving at the oceans (Ockert et al., 2013, Fantle and Tipper, 2014). It then appears essential to identify and characterize Ca elementary and isotopic signatures of these processes to improve our understanding of the mechanisms, which regulate the Ca isotopic signature of the rivers.

In soils, Ca^{2+} has one of the highest affinities for adsorption onto phyllosilicate minerals (Sposito et al., 1983; Tournassat et al., 2004a; 2004b; 2009; Tertre et al., 2013; Lu et al., 2014; Robin et al., 2015). Most often, it is adsorbed as an outer sphere complex, conserving its hydration sphere, and it is bound to the mineral particles by weak and non-specific electrostatic interactions with three different surfaces of phyllosilicate minerals: (1) the basal surface, (2) the edge surface (with aluminol and silanol sites for instance) and (3) the interlayer space when it is accessible (Sposito et al., 1999). Cation adsorption is allowed by phyllosilicate negative charges coming from: (1) isomorphic substitutions within tetrahedral and octahedral layers, leading to permanent negative charge, and (2) deprotonation of sites located on the edge surfaces of the particles, leading to pH-dependent charge (Moore and Reynolds 1989; Thomas, 1996; Mermut and Lagaly, 2001; Bergaya and Lagaly, 2006). The amount of Ca^{2+} adsorbed onto phyllosilicate minerals is relatively well known, and it is described as being dependent on pH, the cationic normality of the environment and the solid/solution ratio (Wahlberg et al., 1965, Levy and Shainberg 1972; McBride, 1994; Liu et al., 1995; Hakem et al., 2000; Missana et al., 2008; Tertre et al., 2011a and b; Lu et al., 2014). Nevertheless, amplitude and nature of Ca isotopic fractionation mechanisms that may occur during adsorption/desorption processes remain poorly studied and understood.

To the best of our knowledge, only one study has dealt with possible isotopic fractionations during Ca adsorption/desorption processes onto clay minerals in a marine environment (Ockert et al., 2013). These authors showed that light isotopes (e.g., ^{40}Ca) were preferentially adsorbed onto clay minerals, and they noticed that the amplitude of associated isotopic fractionation was dependent on the considered clay mineral and the ammonium concentration of their solution. However, the possible link between crystallographic characteristics of minerals and intensity of isotopic fractionation has not been discussed.

The objectives of the present study are to evaluate the effects of crystal chemistry (i.e., layer charge), specific surface area, and interlayer space open to aqueous cations adsorption on Ca isotopic fractionations during adsorption and desorption phenomenon which can occur in continental environments. To do this, adsorption and desorption experiments were carried out onto three well-characterized continental phyllosilicate minerals (i.e., montmorillonite, kaolinite and muscovite). In turn, this helps to improve our understanding of mechanisms that regulate the Ca isotopic compositions of the rivers.

2. MATERIAL AND MEHODS

2.1. Preparation of phyllosilicate minerals

To make a first-order analogy with natural environments, three phyllosilicates that are commonly reported in soils were used in this work (Jackson, 1959; Jackson, 1963; Borchardt, 1989; Fanning et Keramidas, 1989; Dixon, 1989; Douglas, 1989; Mitchell and Soga, 2005). Two well characterized clay minerals (KGa-2 kaolinite and Swy-2 montmorillonite) that are considered to be references in the literature and provided by "The Clay Mineral Society" (www.clays.org, VA, United States of America) were used (Schroth et Sposito, 1997; Ma et Eggleton, 1999; Chipera et Bish, 2001; Guggenheim et Vangroos, 2001; Madejova et Komadel, 2001; Mermut et Cano, 2001; Moll, 2001; Vogt et al., 2002; Dogan et al., 2006). A muscovite, which is one of the major mineral phyllosilicate forming rocks, from the Tuftane region (Norway) provided by the Krantz society (www.krantz-online.de, Bonn, Germany) was also used. These three minerals present different characteristics (CEC, presence or absence of an interlayer space open to hydrated cation adsorption, and layer

147 charge; see Table 1), allowing us to probe the effects of these parameters on Ca
148 adsorption/desorption and subsequent isotopic fractionation.

149 All of the phyllosilicate mineral preparations were carried out at the LhyGeS
150 (Strasbourg, France). The three selected phyllosilicates were prepared at the same low size
151 fraction (i.e., 0.1-1 µm), allowing us to work with minerals (1) that have approximatively the
152 same amount of edge and basal surfaces and (2) that differ only by their layer charge and the
153 accessibility of the interlayer space for aqueous Ca. Note also that most of the mineralogical
154 impurities, such as quartz, are found generally in coarse size fractions (>1 µm) (Vogt et al.,
155 2002). The choice to work with the 0.1-1 µm size fraction also allows us to work with a
156 fraction in which mineralogical impurities are poorly represented. A second coarser size
157 fraction (50-200 µm) of Tuftane muscovite was also prepared to probe the effect of a change
158 of external specific surface area (measured by the BET N_2 method) on elementary
159 adsorption/desorption of Ca and associated isotopic fractionation. To prepare the muscovite
160 size fractions, decametric crystals displaying no visible traces of impurities or alteration were
161 manually transformed into millimetric flakes of 1 cm^2. Then, these were manually grinded in
162 deionized water using an immersion blender (SLIMFORCE SEB^{TM}) to obtain fine particles
163 (0-200 µm). The 50-200 µm size fraction of Tuftane muscovite was recovered by wet sieving,
164 while the remaining size fraction (0-50 µm) was reserved.

165 To obtain the 0.1-1 µm size fraction of each selected phyllosilicates, one gram of
166 powder (as-received KGa-2 and Swy-2 and the 0-50 µm size fraction for muscovite) was
167 immersed in 50 mL of distilled water (18.2 $m\Omega.cm^{-1}$) and mixed with a deflocculant (Tetra-
168 sodiumdiphosphate-10-hydrate) at a low concentration (0.01 $mol.L^{-1}$) to avoid aggregate
169 formation. After 24 hours of stirring at 40 rpm on a SB3 Stuart^{TM}, the size separation was
170 performed according to Stokes' law applied to centrifugation steps, allowing the elimination
171 of the particles with sizes out the 0.1-1 µm range (see Reinholdt et al., 2013). These

centrifugations were carried out on a ThermoScientific Heraus Megafuge 40R^{TM} centrifuge and a Beckman Coulter Avanti J-30I^{TM} ultracentrifuge instrument. The 0.1-1 µm size fractions of each mineral obtained in wet conditions were dried in an oven at 60°C and stored.

To investigate a single cation pair exchange (Ca^{2+} to Na^{+}), all the phyllosilicate mineral size fractions were conditioned in sodium-homoionic form. For each mineral, 0.25 g of powder was stirred with 50 mL of 1 mol.L^{-1} NaCl (99.99% purity) solution for nine days. Every three days, the supernatant was replaced by a fresh NaCl solution to remove desorbed elements, and an intermediate step was performed with a NaCl solution at pH=3 (addition of HNO_3) to decarbonate the samples. The samples were then dialysed for five days to eliminate all the non-adsorbed elements: 200 mL of suspension (NaCl + phyllosilicate minerals) were equilibrated with 1.5 L of distilled water, which was renewed every 24 h until complete Cl^- elimination. All the size fractions were then dried in an oven at 60°C for three days and were manually and gently crushed in an agate mortar to disaggregate them.

2.2. Characterization of prepared phyllosilicate minerals

Effectiveness of the mineral preparation was confirmed by three types of measurements performed on the final obtained fractions: **(1)** Powder X-ray diffraction (XRD) analysis using a Bruker AXS D5000 diffractometer at the LhyGeS (Strasbourg, France) was carried out in θ/θ mode by scanning between 3° and 65° with steps of 0.04° every 10 sec. Acquisition was obtained using an X-ray tube equipped with a copper (Cu) anticathode operating at 40 kV and 30 mA. **(2)** Cation exchange capacity (CEC) was measured using the hexaamine-cobalt method described by Ciesielski et al. (1997): 100 mg of powder was mixed with 40 mL of 10^{-3} mol.L^{-1} chloride hexaamine-cobalt solution for two hours at 40 rpm on a SB3 Stuart^{TM} rotator at room temperature. The suspensions were then filtered at 0.45 µm

using regenerated cellulose filters and elementarily analysed using a ThermoScientific iCAP 6000series™ ICP-AES (inductively coupled plasma atomic emission spectrometer) at the LHyGeS (Strasbourg, France). **(3)** External specific surface area measurements were performed on a Micrometrics Tristar™ at IC2MP (Poitiers, France) according to the Brunauer-Emmett-Teller (BET) method (Brunauer et al., 1938) using the N_2 adsorption isotherm. Morphologies of basal surfaces of the Tuftane muscovite grains at two different sizes (50-200 µm and 0.1-1 µm) were also checked with a Tescan Vega 2 scanning electron microscope (SEM) at the LHyGeS (France).

The CEC and BET N_2 specific surface area values measured in this work are presented in Table 1. These values are on the same order of the previously published data for KGa-2 and Swy-2 (see Borden and Giese, 2001; Kosmulsky, 2009; and references therein). As expected, for Tuftane muscovite, the BET N_2 specific surface area and the CEC are strongly dependent on the grain size fraction and the basal and edge surfaces proportions (Osman and Suter, 2000; Sivamohan and Vachot, 1990). For each mineral investigated, the percentages of the CEC represented by Na ions were also calculated (see Table 1), and they are higher than 90%, indicating that the Na-homoionic conditioning was effective in every case.

2.3. Cation-exchange experiments

Adsorption and desorption experiments were carried out with "solution-mineral" batch-systems. Ca concentrations in the initial solution (see Table 2) were adjusted for each batch system to have Ca consumption superior to 75%, simultaneously leading (1) a sufficient amount of adsorbed Ca for performing isotopic measurements and (2) a limiting solution (i.e.,

221 the initial amount of Ca is non-infinite with respect to the amount of adsorbed Ca), making it
222 possible to resolve the isotopic fractionation with a high resolution. .

223 For each size fraction, adsorption/desorption experiments were carried out up to 48
224 h with ten time steps, including five minutes of centrifugation: 5 min, 10 min, 15 min, 20 min,
225 35 min, 65 min, 125 min, 425 min (~7 h), 1445 min (~24 h) and 2885 min (~48 h).
226 Experiments were performed at pH=4 and pH=7, typical pH values for soil under a temperate
227 climate and forested soils (McCauley et al., 2009), at room temperature (20°C), at a 2.5 $g.L^{-1}$
228 solid/solution ratio, and without background salt [ionic strength is fixed solely by the
229 $Ca(NO_3)_2$ and reagents used to adjust the pH of initial solution]. Each measurement point
230 represents a single and separate experiment.

231 Each batch experiment consisted of mixing 100 mg of each mineral with 40 mL of
232 initial Ca solution at the considered pH (adjusted by addition of $5x10^{-2}$ N HNO_3 or $5x10^{-3}$ N
233 NaOH solutions). Each mixture was shaken at 40 rpm on a SB3 Stuart™ rotator. At the
234 selected time, KGa-2 and Tuftane muscovite samples were centrifuged for 5 min at 4000 rpm
235 in a Thermo Jouan multifunction B4-I™ centrifuge, and Swy-2 samples were centrifuged at
236 17000 rpm (due to possible swelling) in a Beckman Coutler Avanti J-30I™ ultracentrifuge
237 instrument, respectively. To measure both Ca elementary and isotopic compositions after
238 adsorption experiments, the supernatant was removed using a 20 mL syringe and filtered at
239 0.2 µm using cellulose acetate membrane filters. The evolution of pH with time was measured
240 on an aliquot of each filtered sample using a Metrohm 905 Titrando™ titrator calibrated at
241 25°C.

242 For desorption, the residue (i.e., clay slurry remaining after supernatant removal) of
243 each tube was weighed to quantify the residual liquid mass. The clay slurry was stirred with
244 20 mL of a chloride hexaamine-cobalt solution whose concentration was dependent on the
245 CEC of the mineral [10^{-4} $mol.L^{-1}$ for KGa-2 and Tuftane muscovite (50-200 µm), 10^{-3} $mol.L^{-1}$

for Tuftane muscovite (0.1-1 µm), and 10^{-2} mol.L^{-1} for Swy-2; see Table 3]. After 24 h of stirring at 40 rpm on a SB3 Stuart^{TM} rotator, the desorption was considered as complete (no evolution of the desorbed Ca amount was measured in the laboratory after 24 h), and each tube was centrifuged at 4000 rpm for 5 min on a Thermo Jouan multifunction B4-I^{TM} centrifuge instrument. The same procedure of filtration as that used for the adsorption experiments was applied.

To measure the effect of other cations' presence in solution on the amount of Ca adsorbed or desorbed and the associated isotopic fractionation, other experiments were carried out for KGa-2 and Swy-2 by following the same protocol presented above. These specific experiments were performed for 120 min at pH=7, which are conditions under which a chemical stationary state is reached (see results section). The effects of cationic competition were tested by adding K^+, Sr^{2+}, and Mg^{2+}, all in nitric form (Alfa Aesar Puratronic^{TM}), to the $Ca(NO_3)_2$ initial solution. Aqueous concentrations of K^+, Sr^{2+}, and Mg^{2+} were calculated to allow saturation of all adsorption sites [Test (1)], half of the adsorption sites [Test (1/2)] and a quarter of the adsorption sites [Test (1/4)] present on the mineral, assuming that each of the considered cations was susceptible to saturate the adsorption sites. Moreover, the effects of ionic strengths were tested by adding decreasing concentrations of NaCl (99.99%, Alfa Aesar^{TM}) to a $Ca(NO_3)_2$ initial solution, from 10^{-1} mol.L^{-1} (Test 10^{-1}) to 10^{-2} mol.L^{-1} (Test 10^{-2}) and to 10^{-3} mol.L^{-1} (Test 10^{-3}) (see Table 4).

2.4. Analytical procedures

The amount of Ca potentially present in each mineral (exchangeable or structural) before adsorption/desorption experiments was elementarily measured, and its isotopic signature was determined. The four mineral size fractions were dissolved in Savillex^{TM}

beakers by an acid oxidative digestion procedure classically used at LhyGeS (Chabaux et al., 2013; Pelt et al., 2013). This process consists of the digestion of 100 mg of grinded sample by successive acid baths (HF-HNO_3, $HClO_4$ and HCl-H_3BO_3) to achieve complete dissolution of the samples. The samples were then evaporated to dryness, dissolved in 10 mL of 0.5 N HNO_3, and stored for chemical and isotopic analysis. The total Ca blank from this digestion procedure (i.e., the Ca release from reagents, the vessel, and the methods used) was less than 50 ng, which represents less than a 0.01% contribution to the Ca from samples. Thus, this contribution will be neglected in the calculations reported in the next sections.

All elementary analyses presented in this work were performed on a ThermoScientific iCAP 6000series^{TM} ICP-AES (inductively coupled plasma atomic emission spectrometer) at the LhyGeS (Strasbourg, France) with an accuracy between 3% and 10% [depending on the element (Dequincey et al., 2006)]. To perform Ca isotope measurements, a mixture formed from 0.14 µmol of Ca of each sample and 0.01 µmol of ^{42}Ca-^{43}Ca double spike [^{42}Ca/^{43}Ca spike ratio of ~5, following Holmden, (2005)], corresponding to a ^{40}Ca/^{42}Ca ratio of ~16 in the spiked sample, was dried at 90°C on a hot plate and then dissolved in 2 N HNO_3 before Ca separation. All samples and internal standard (Atlantic seawater, Schmitt et al., 2001; Hippler et al., 2003) solutions were loaded into ion-exchange chromatographic columns (high density polyethylene) filled with 2 mL of DGA normal resin (TODGA) from Triskem^{TM} (Horwitz et al., 2005; Romaniello et al., 2015). This resin has a high retention capacity for Ca and Sr and no affinity to other major cations in a weakly concentrated nitric condition (Horwitz et al., 2005). These characteristics make effective the elimination of the matrix and the potential interfering elements (in particular Sr, K, Fe, and Al) (Fig. 1). After the Ca elution procedure (~100% of Ca eluted), all the samples were dried a first time at 90°C and then converted into nitric form by the addition of 2 mL of 7 N HNO_3 before a second drying at 90°C on a hot plate. Note that the total Ca blank for this separation represents less

than a 0.2% contribution to the Ca from samples. Thus, as for the digestion procedure, this contribution will be neglected in the calculations reported in the next sections.

Then, each sample was dissolved in 1-3 µL of 1 N HNO_3 and deposited on a tantalum single filament (99.995% purity), previously degassed and oxidized under primary vacuum. Calcium isotope measurements were performed at the LHyGeS (Strasbourg, France) with a ThermoScientific Triton^{TM} TIMS (thermo-ionization mass spectrometer) in dynamic multi-collection mode, following the methods described by Schmitt et al. (2009, 2013). Measured values were expressed as $\delta^{44/40}$Ca in per mil relative to the NIST SRM915a standard (Hippler et al., 2003; Eisenhauer et al., 2004):

$$\delta^{44/40}Ca(‰) = \left(\frac{\frac{^{44}Ca}{^{40}Ca}_{Sample}}{\frac{^{44}Ca}{^{40}Ca}_{standard}} - 1 \right) \times 1000 \qquad (1)$$

Our Ca isotopic results will be discussed in terms of variations with respect to initial solution isotopic signature (apparent isotopic fractionation; $\Delta^{44/40}Ca_{MAA\ or\ MAD}$), as follows:

$$\Delta^{44/40}Ca_{MAA\ or\ MAD} - \delta^{44/40}Ca_{MAA\ or\ MAD} - \delta^{44/40}Ca_{IS} \qquad (2)$$

where $\delta^{44/40}Ca_{MAA}$ and $\delta^{44/40}Ca_{MAD}$ are the isotopic signatures of the supernatant measured after adsorption experiments, respectively, and $\delta^{44/40}Ca_{IS}$ is that of the initial solution ($\delta^{44/40}Ca_{IS}$= 0.79‰ ± 0.03‰, 2SE, N=16). Standard error (i.e., 2SE) is used in that case to estimate the error of the mean of a data population measured numerous times (i.e., $\delta^{44/40}Ca_{IS}$). This statistic treatment is recommended to compare the mean of large data populations with large dispersion (Altman and Bland, 2005). For samples measured one or two times, we use the standard deviation (2SD) given by the dispersion of the standards (i.e., 0.11‰, see next

paragraph). To avoid underestimating our uncertainty, when the values of the dispersion of the standards (in 2SD) are lower than the errors on the measured samples (in 2SE), the latter are used.

The uncertainties associated with $\Delta^{44/40}Ca_{MAA\ or\ MAD}$ values was determined following an uncertainty propagation calculation for sum:

$$\Delta_{(\Delta^{44/40}Ca_{MAA\ or\ MAD})} = \sqrt{\left(\Delta_{(\delta^{44/40}Ca_{MAA\ or\ MAD})}\right)^2 + \left(\Delta_{(\delta^{44/40}Ca_{IS})}\right)^2} \qquad (3)$$

where $\Delta_{(\Delta 44/40CaMAA\ or\ MAD)}$, $\Delta_{(\delta 44/40CaMAA\ or\ MAD)}$, and $\Delta_{(\delta 44/40CaIS)}$ are the uncertainties associated to $\Delta^{44/40}Ca_{MAA\ or\ MAD}$, $\delta^{44/40}Ca_{MAA\ or\ MAD}$, and $\delta^{44/40}Ca_{IS}$, respectively.

The average external reproducibility of $\delta^{44/40}Ca$ measurements was 0.11‰ based on repeated measurements of NIST SRM915a (2SD, N=20) and 0.10‰ based on sample replicate measurements (2SD, N=25). The highest value was chosen as the external reproducibility (i.e., 0.11‰) in this study. The accuracy of our measurements was explored through the measurements of an internal Atlantic seawater standard (1.85‰ ± 0.11‰, 2SD, N=34) during the same period, which showed consistent values with those reported by Hippler et al. (2003), Heuser et al. (2016) and the references therein.

3. RESULTS

3.1. Mass balance of adsorption-desorption

Ca adsorption and desorption were constrained by Ca elemental and isotopic analysis of the filtered supernatant obtained at the end of the adsorption and desorption procedures. The amounts of Ca adsorbed onto the minerals were thus calculated by subtracting the amount of Ca measured in the supernatant after adsorption experiments to the Ca amount in the initial solution. All adsorption results are presented in Tables 2 and 4, and the desorption results are presented in Tables 3 and 4.

The filtration process is never 100% efficient and minerals are never entirely dried, indicating that a certain volume of the initial solution (that has reacted with the solid) remains in the pores of the mineral as residual liquid, which cannot be experimentally avoided: drying can cause salt precipitation and washing can create a new uncontrolled cation exchange. For desorption experiments, a chloride hexaamine-cobalt solution is added to the residue of adsorption (mineral + residual liquid = slurry). The Ca amounts present in the residual fluid and the initial chloride hexaamine-cobalt solution may modify elemental and isotopic signatures of the supernatant recovered after the desorption experiments. The Ca proportions coming from the residual liquid in clay slurry and the hexaamine-cobalt solution are reported in Tables 3 and 4. The tables report also isotopic signatures characterising Ca desorption (i.e., $\Delta^{44/40}Ca_{MAD}$), corrected or not, from these contributions. Applied corrections were not significant in both elementary and isotopic results, and they will no longer be considered in this article. Detailed calculations are available in the supplementary materials.

The results reported in Table 3 have not been corrected by the contribution of the possible dissolution of the mineral during adsorption/desorption experiments. For both KGa-2 and Tuftane muscovite, this assumption was justified, since no Ca was measured in the solution issued from their acidic digestion (section 2.4.). As far as Swy-2 is concerned, the acidic digestion experiment led to 1.75 µmol of Ca per 0.1 g, an amount corresponding to only 5% of the amount of Ca in the initial solution if all of the solid is digested. In our

experiments at pH=4, only 0.6% of the solid was digested in 48 h, corresponding to 0.03% of Ca amount in the initial solution. This contribution was calculated by using aqueous silica measured in the supernatant after adsorption at pH=4 and by assuming a stoichiometric dissolution of the mineral. Thus, even if the release of alkali/alkaline earth ions can occur in the first steps of the experiments performed at pH=4 due to aluminosilicate dissolution (see Oelkers et al., 1994), we can reasonably assume that this contribution will be negligible, considering the very slight dissolution measured (0.6 wt% of the solid in 48 h). Thus, we will neglect dissolution of Swy-2 in our experiments and also its potential contribution to Ca elementary and isotopic compositions of the solution.

The Ca adsorbed isotopic signature can be calculated by following the equation:

$$\Delta^{44/40}Ca_{ADS} = \frac{\left(\Delta^{44/40}Ca_{IS}\right) - \left(\Delta^{44/40}Ca_{MAA} \times (1-p)\right)}{p} \qquad (4)$$

where $\Delta^{44/40}Ca_{ADS}$, $\Delta^{44/40}Ca_{IS}$ and $\Delta^{44/40}Ca_{MAA}$ are the Ca isotopic signatures of the adsorbed Ca, the initial solution and the supernatant measured after adsorption experiments, respectively. *p* is the proportion of the initial Ca adsorbed onto minerals. Note that in our case, $\Delta^{44/40}Ca_{IS}$ is equal to 0. By considering total desorption, calculated $\Delta^{44/40}Ca_{ADS}$ should be on the same order as $\Delta^{44/40}Ca_{DES}$ (the isotopic value of desorbed Ca) and measured and corrected $\Delta^{44/40}Ca_{MAD\ corrected}$ (the isotopic value of the supernatant measured after desorption experiments) (see section 4.3.). The performed calculations have validated that our experiments follow the mass balance within the error bars (see supplementary materials).

Our experiments were carried out under atmospheric conditions, allowing CO_2 dissolution during adsorption experiments. The calculation, performed with VisualMinteq™ version 3.1 software associated with the "thermo.vbd" thermodynamic database (Gustafsson, 2013), showed that all solutions recovered after adsorption and desorption experiments are

strongly undersaturated with respect to calcite, suggesting that $CaCO_3$ precipitation was not possible in our experiments. Thus, this process will be neglected in the discussion reported in the next sections relative to amounts of adsorbed Ca and the associated isotopic fractionation.

3.2. Adsorbed and desorbed Ca amounts evolution through time

Considering Ca adsorption, similar trends are observed in the supernatant recovered after the elemental adsorption on KGa-2 at pH=7, Tuftane muscovite (50-200 µm) at pH=7, and Swy-2 and the Tuftane muscovite (0.1-1 µm) at pH=4 and pH=7 (Fig. 2B, 2D-H). A rapid decrease in the supernatant Ca content, which implies a rapid increase of the adsorbed Ca amount onto minerals, is observed initially in the experiment, and a maximum of adsorption is reached after: (1) 15 min for KGa-2 and Tuftane muscovite (50-200 µm) at pH=7; (2) 35 min for Tuftane muscovite (0.1-1 µm) at pH=4 and pH=7; and (3) 65 min for Swy-2 at pH=4 and pH=7. In all cases, maxima of adsorption were followed by the establishment of a chemical stationary state with amounts of adsorbed Ca that no longer evolved up to 48 h (i.e., 2880 min).

Concerning KGa-2 experiments at pH=4, the Ca adsorption rate decreases with time from 15 min to 48 h (Fig. 2A), which could be explained by a $2H^+$-Ca^{2+} cation exchange taking place after 10 min of reaction. Such an exchange cannot be experimentally measured because the amount of H^+ exchanged with Ca^{2+} necessary to explain the difference in the adsorbed Ca amount (see Table 2) will only generate a 0.02 pH unit decrease, which is within the analytical error of the pH-meter used (±0.2 pH unit). In the case of the Tuftane muscovite (50-200 µm), no Ca adsorption was observed (Fig. 2C).

The amounts of desorbed Ca for each mineral are also presented in Fig. 2. The amounts of Ca measured in the supernatant recovered after desorption experiments were

417 between 97% ± 5-10% and 103% ± 5-10% of the Ca amount adsorbed on each mineral (Table
418 3), indicating that almost all of the adsorbed Ca was desorbed and suggesting a reversible
419 process.

420 If we now consider the cationic competition experiments, we observe that the
421 percentage of adsorbed K remains constant no matter the test and slightly higher for Swy-2
422 than for KGa-2 (22% and 27-30%, respectively, Table 4). In contrast, the percentages of
423 adsorbed Ca, Sr and Mg increase from Test (1) to Test (1/4), with approximately 70% of each
424 element being adsorbed, no matter the considered mineral. In contrast, if Ca and Sr
425 desorptions are complete, no matter the test or the mineral, desorptions of K and Mg are not,
426 and their effectiveness increases from Test (1) to Test (1/4) for both KGa-2 and Swy-2, with
427 maxima at 50% and 4% for K and Mg, respectively. As far as the effect of ionic strength is
428 concerned, adsorbed Ca concentrations are inversely correlated with the NaCl concentrations
429 of the initial solutions of both KGa2 and Swy-2 (Table 4). The desorption procedure is in all
430 cases complete, indicating a reversible Ca adsorption.

431

432 ### *3.3. Evolution of Ca isotopic fractionation during adsorption and*
433 ### *desorption*

434

435 The $\Delta^{44/40}$Ca values calculated (see section 2.4.) after adsorption experiments
436 evolved as a function of the studied mineral (see Fig. 3). No evolution of isotopic values
437 through time was observed for KGa-2 at pH=4 and pH=7 and for Tuftane muscovite (50-200
438 µm) at pH=7 (Fig. 3A, 3B, and 3D). Note that no isotopic measurements were performed on
439 the experiments carried out with the 50-200 µm size fraction of Tuftane muscovite at pH=4
440 due to the lack of Ca adsorption in these conditions (see Fig. 2C). By contrast, a constant
441 apparent Ca isotopic fractionation of +0.22-0.27‰ was measured in the supernatant after Ca

adsorption onto Tuftane muscovite (0.1-1 µm) at both pH values, up to 24 h (Fig. 3E and 3F), indicating an isotopic stationary state with a preferential uptake of light isotopes (e.g., ^{40}Ca) during Ca adsorption.

A different trend was observed for Swy-2 at both pH values (Fig. 3G and 3H). First, a rapid increase in $\Delta^{44/40}Ca$ was observed during the first 20 min, with a maximum isotopic fractionation of +0.24-0.29‰ (for pH=7 and pH=4, respectively). Later, the $\Delta^{44/40}Ca$ decreased somehow to remain constant for both pH values, at approximately 0.10‰ higher than the initial solution.

If we now consider results from cationic competition experiments as well as the effect of the ionic strength (Fig. 4) and even if an isotopic trend seems to appear during Swy-2 adsorption experiments (an increase of $\Delta^{44/40}Ca_{MAA}$ when other cation concentrations decrease; R^2=0.9772 and R^2=0.9326, for competition and ionic strength, respectively), no significant Ca isotopic fractionation can be observed for KGa-2 at pH=7. This trend cannot be discussed with sufficient robustness due to the very low isotopic fractionation generated.

For all materials investigated, the $\Delta^{44/40}Ca_{MAD}$ values calculated after the desorption experiments (Fig. 3 and 4) from our measured $\delta^{44/40}Ca_{MAD}$ values (see Eq. 2) were equal to zero within analytical uncertainties. These values can be compared to those calculated (e.g., $\Delta^{44/40}Ca_{DES}$) following the mass balance equation presented in section 3.1 (see Eq. 4) using the $\Delta^{44/40}Ca_{MAA}$ and $\Delta^{44/40}Ca_{IS}$ measured values, and the proportion of Ca adsorbed (i.e., *p*). These results indicate that, even if the Ca adsorbed on the mineral should has a lower isotopic signature than the Ca remaining in the supernatant after adsorption, this theorical isotopic fractionation is too slight in our conditions to be measurable on the desorbed Ca (see section 4.3).

4. DISCUSSION

4.1. Factors controlling adsorption

Three types of adsorption sites are present in different proportions on phyllosilicate minerals: the edge surfaces (pH-dependent sites), the basal surfaces, and the interlayer space (both pH-independent site; Sposito et al., 1999). Contrary to Swy-2 (montmorillonite), Ca adsorption only takes place on basal and edge surfaces of KGa-2 (kaolinite) and Tuftane muscovite, as their interlayer spaces remain inaccessible to aqueous cation adsorption due to, respectively: (1) hydrogen bonds, which remain stable in water (Mitchell and Soga, 2005), and (2) strongly fixed K^+, which cannot be mobilized by another cation under our experimental conditions. Note that no extra K were measured in the supernatant recovered after the adsorption experiments, confirming the latter. The recorded amounts of adsorbed Ca is different across the experiments, which can be linked to the proportion of different adsorption sites of each mineral and the grain-size fraction used.

Kaolinite is considered as a mineral without isomorphic substitution of Si and Al in tetrahedral or octahedral layers, which lead to an absence of pH-independent negative layer charge (0/cell; Ferris and Jepson, 1975; Sposito, 2008). Thus, Ca adsorption onto KGa-2 can only take place on edge surfaces whose protonation state is pH-dependent.

Like KGa-2, the reactive surface of Tuftane muscovite (50-200 µm) is totally pH-dependent, and it was certainly represented only by edge surface sites during our experiments in which no Ca adsorption was measured at pH=4 and a low Ca amount was adsorbed at pH=7 (probably due to deprotonation of silanol sites at this pH; Tertre et al., 2006). Thus, high layer charge of muscovite (2/cell; Guggenheim et al., 2006) does not lead to an important adsorption onto the basal surface (to compensate for permanent negative layer

charge) at this grain size. This effect can be explained by the very low specific surface area of the mineral (<0.1 $m^2.g^{-1}$), which lead to a very small amount of reactive adsorption sites, particularly basal surfaces. In contrast, a large amount of Ca was adsorbed at both pH values for Tuftane muscovite (0.1-1 µm), and a low difference in the adsorbed Ca amount between pH=4 and pH=7 was recorded, pointing to a small amount of pH-dependent reactive surfaces (edge surfaces) and a large amount of pH-independent reactive surfaces (basal surfaces), in agreement with the important specific surface area measured for this grain-size fraction (62.23 $m^2.g^{-1}$; see Table 1).

The difference in basal site proportion observed between the two studied grain size fractions of Tuftane muscovite is linked to the grinding process, which causes a size reduction without necessarily preserving the proportions of each type of adsorption site (MacKenzie and Milne, 1953; Papirer et al., 1986; Sivamohan and Vachot, 1990). Two main types of size reductions are recorded: (1) fractures perpendicular to the (001) faces, which allow formation of new edge surfaces by breaking crystalline layer tetrahedrons and octahedrons, and (2) delamination along the (001) faces, which allow an increase in the proportion of basal surfaces (Sivamohan and Vachot, 1990; Parez-Maqueda et al., 2003; see Fig. 5). These two combined effects explain the increase in the absolute number of available sites (and particularly of basal surface sites) for adsorption when the particle size decreases, and they are therefore compatible with a significant difference in the of CEC and the external specific surface area between the two size fractions (see Table 1).

The same amounts of Ca are adsorbed onto Swy-2 at pH=4 and pH=7 (see section 3.2.), implying a solely pH-independent site contribution, which is in agreement with the H^+ saturation of the Swy-2 edge surface sites in our experimental conditions (Tertre et al., 2011b). Thus, Na^+-Ca^{2+} exchange occurs only on basal surfaces (to compensate for the permanent negative layer charge, 0.6/cell; Guggenheim et al., 2006) and in interlayer spaces.

The latter mobilizes Ca rapidly, as seen by the amount of adsorbed Ca on Swy-2 (basal surface sites and interlayer space sites), which is five times greater than the amount onto Tuftane muscovite (0.1-1 µm) (majority of basal surface sites). This difference cannot be explained only by the external specific surface area difference [28.60 and 62.23 for Swy-2 and Tuftane muscovite (0.1-1 µm), respectively; see Table 1] and it implies adsorption in internal sites as interlayer space sites for Swy-2.

Beyond pH-dependence of adsorption sites, the contact time between Ca initial solution and minerals plays an important role in the adsorption amount and in the establishment of an adsorption stationary state. The latter is related to: (1) the time needed to reach the adsorption site (especially by diffusion into the interlayer space; Tertre et al., 2015) and (2) the mineral CEC (the higher CEC implies more time is needed to reach a stationary state; see Fig. 6). Thus, the differences in time needed to reach the elementary stationary state observed for Tuftane muscovite (50-200 µm), KGa-2, Tuftane muscovite (0.1-1 µm) and Swy-2 can be explained by their differences of the permanent negative layer charge (which leads to adsorption on the basal surfaces), the specific surface area (i.e., amount of available adsorption sites) and the contribution of interlayer spaces (i.e., important amount of internal adsorption site).

4.2. Ca isotopic fractionation pattern during adsorption

No isotopic fractionations were measured during the KGa-2 and Tuftane muscovite (50-200 µm) experiments, in which only edge surface sites are involved in Ca adsorption. This result indicate that edge surface sites do not generate isotopic fractionation during Ca adsorption, implying that ^{40}Ca and ^{44}Ca isotopes are equally adsorbed. With regard to Tuftane muscovite (0.1-1 µm), for which adsorption occurs for the most part on basal surfaces, a

positive isotopic fractionation plateau (+0.24‰) was reached in the supernatant after 10 min of adsorption experiments at both pH values. These results indicate that basal surface sites are rapidly reached by Ca in solution and that they are highly selective for the light isotopes of Ca (e.g., ^{40}Ca). A different pattern of positive isotopic fractionation was recorded during the Swy-2 experiments, in which adsorption occurred on basal surfaces and in interlayer spaces. A high isotopic fractionation (+0.24‰ to 0.29‰) was measured in the supernatant until 65 min of reaction had passed, after which values decreased, with an isotopic plateau forming at a value of +0.10‰ for up to 48 h at both pH values. These different behaviours of Tuftane muscovite (0.1-1 µm) and Swy-2 can be explained by the adsorption on the interlayer space sites, which also have high selectivity for light isotopes of Ca (e.g., ^{40}Ca) and play an important role during the first 65 min of Swy-2 experiments. Adsorption onto basal surfaces of Swy-2 can explain the isotopic plateau recorded after 65 min of reaction, which presents the same pattern as the one observed during Tuftane muscovite (0.1-1 µm) experiments. Thus, Ca isotopic fractionation during adsorption is site-dependent, and it is controlled by adsorption on basal surfaces and in interlayer spaces. Moreover, the same intensities of isotopic fractionation were recorded at both pH values for each mineral, indicating that contrary to elementary adsorption, Ca isotopic fractionation intensity is pH-independent.

The $\Delta^{44/40}$Ca mean values calculated for the last recorded times of the adsorption experiments (i.e., isotopic plateau) increased from KGa-2 (0‰) to Swy-2 (+0.10‰) and Tuftane muscovite (+0.24‰). By assuming that the isotopic fractionation recorded during the isotopic plateau is generated by adsorption onto basal surfaces, the mineral layer charge can explain the gradual increase of the Ca isotopic fractionation from KGa-2 (0/cell) to Swy-2 and Tuftane muscovite (0.6/cell and 2/cell, respectively). As no Ca isotopic fractionations were recorded during the Tuftane muscovite (50-200 µm) experiments despite a high layer charge, we assume that the grain size fraction and thus the specific surface area of the mineral must be

567 important for generating isotopic fractionation during adsorption. Thus, the Ca isotopic
568 fractionation intensity is controlled by: (1) the layer charge and the surface specific area
569 (grain size fraction) of the mineral and (2) the presence of an interlayer space open to
570 hydrated cation adsorption.

571 Mean values and associated 2SE errors have been calculated for the isotopic plateau
572 (i.e., isotopic stationary state) recorded during the Swy-2 and Tuftane muscovite (0.1-1 µm)
573 experiments at pH=4 and pH=7. These values were used to calculate the isotopic fractionation
574 factor (i.e., $\alpha_{IS\text{-}MAA}$) between supernatant recovery after the adsorption experiments (i.e.,
575 $\Delta^{44/40}Ca_{MAA}$) and the initial solution (i.e., $\Delta^{44/40}Ca_{IS}$) for both minerals, as follows:

576

$$\alpha_{IS-MAA} = \frac{\Delta^{44/40}Ca_{IS} + 1000}{\Delta^{44/40}Ca_{MAA} + 1000} \qquad (5)$$

577

578

579 By considering the error associated with each $\Delta^{44/40}Ca_{MAA}$ mean value, these calculations lead
580 to an interval of α values for each mineral at both pH values: (1) $\alpha_{IS\text{-}MAA}$=0.99973 to 0.99979
581 and 0.99975 to 0.99978 for Tuftane muscovite (0.1-1 µm) at pH=4 and pH=7, respectively;
582 (2) $\alpha_{IS\text{-}MAA}$=0.99985 to 0.99996 and 0.99989 to 0.99992 for Swy-2 at pH=4 and pH=7,
583 respectively (see Fig.7).

584 These isotopic fractionation factors were then used to calculate theoretical
585 $\Delta^{44/40}Ca_{MAA}$ values following a closed system equilibrium law described by:

586

$$\Delta^{44/40}Ca_{MAA} - \Delta^{44/40}Ca_{IS} + (f \times \varepsilon) \qquad (6)$$

587

$$\varepsilon = (\alpha_{IS-MAA} - 1) \times 1000 \qquad (7)$$

588

589

590 where $\Delta^{44/40}Ca_{IS}$ is the isotopic value of the initial solution (i.e., 0‰), *f* is the fraction of Ca
591 remaining in the solution after the adsorption experiments, and $\alpha_{IS\text{-}MAA}$ is the isotopic
592 fractionation factor reported above for Tuftane muscovite (0.1-1 µm) and Swy-2 at both pH
593 values.

594 In the cases of the Tuftane muscovite (0.1-1 µm) at both pH values, and Swy-2 at
595 both pH values in adsorption experiments from 65 min up to 48 h (i.e., more than 90% of
596 initial Ca adsorbed), the measured values of Ca isotopic fractionation follow a closed system
597 equilibrium fractionation law. A similar trend has been observed for other elements (Li and
598 Cu) adsorbed onto clay minerals, and it has been explained, for metallic cations, by a
599 differential adsorption of aqueous chemical species involving the studied element (e.g., Millot
600 and Girard, 2007; Li et al., 2015 and references therein). Despite the robustness of this
601 explanation for results reported in these previous studies, it is highly unlikely in our case,
602 since the first main aqueous Ca species (Ca^{2+}) is, at least, one thousand times more
603 concentrated than the second one ($CaNO_3^+$) (as calculated using VisualMinteq^{TM} version 3.1
604 software associated with the "thermo.vbd" thermodynamic database; Gustafsson, 2013). The
605 only common factor between Swy-2 and Tuftane muscovite (0.1-1 µm) is the layer charge,
606 which differs in intensity. Thus, the adsorption onto the basal surface should control the
607 recorded isotopic fractionation at thermodynamic equilibrium. Moreover, layer charge
608 intensity could imply a higher selectivity for light isotopes (e.g., ^{40}Ca) for basal surface sites,
609 which explain the isotopic fractionation intensity difference between the two minerals
610 [+0.24‰ to +0.10‰ for Tuftane muscovite (0.1-1 µm) and Swy-2, respectively].

611 Within the first 35 min of Swy-2 adsorption experiments (i.e., less than 90% of Ca
612 adsorbed), Ca isotopic fractionation does not follow a closed system equilibrium law,
613 indicating that other processes are necessary to explain our measured values (see Fig. 7C and
614 7D). By assuming the Swy-2 interlayer space is a finite space box, a selective adsorption of
615 light Ca isotopes (e.g., ^{40}Ca), with no back-reaction, could generate an increase of

616 $\Delta^{44/40}Ca_{MAA}$ until an isotopic plateau corresponding to the maximum Ca adsorption capacity
617 of the interlayer space is attained (Fig. 8A). This unidirectional adsorption of light Ca isotopes
618 thus generates a kinetic isotopic fractionation when the adsorption reaction first occurs, which
619 eases when the maximum capacity of Ca adsorption in the interlayer space is reached. A
620 decrease of $\Delta^{44/40}Ca_{MAA}$ isotopic values could then be generated by complete (i.e.,
621 $\Delta^{44/40}Ca_{MAA} = \Delta^{44/40}Ca_{IS}$) or incomplete (i.e., $\Delta^{44/40}Ca_{MAA} > \Delta^{44/40}Ca_{IS}$) equilibration of the
622 interlayer space with the surrounding solution (see Fig.8 B).

623 Thus, $\Delta^{44/40}Ca_{MAA}$ measured during our experiments should be the result of three
624 phenomena: (1) a kinetic isotopic fractionation due to preferential adsorption of light isotopes
625 into the interlayer space, (2) an isotopic equilibration of the interlayer space with the
626 surrounding solution, and (3) an equilibrium fractionation linked to the intensity of the layer
627 charge. The last phenomena should be the principal contributor of $\Delta^{44/40}Ca_{MAA}$ after 65 min of
628 reaction if the isotopic equilibration is complete (see Fig. 8C and 8D).

629

630 ### *4.3. Implications for other phyllosilicate minerals commonly found*
631 ### *within soils*

632

633 Many phyllosilicate minerals, particularly clay minerals, are represented within
634 natural soils. Their proportions are extremely variable and dependent on parameters driving
635 weathering and pedogenesis: (1) the substratum forming the soil, (2) climatic conditions (e.g.,
636 temperature and precipitation), (3) the chemical composition of the soil solution, and (4)
637 biological activities (Wilson, 1999; Meunier, 2005). Our controlled parameters (especially the
638 Ca concentration of the initial solution and the solid/solution ratio) and the small number of
639 quantitative data available in the literature about phyllosilicate mineral proportions within
640 soils make difficult the transposition of the results obtained in this study to natural

environments. Nevertheless, the potentially very high solid/solution ratio of natural soil [from zero to several kilograms of clay mineral per litre of soil solution, calculated from Weil and Brady (2017)] could, in the light of current knowledge, generate a Ca-limiting solution (i.e., more than 75% of Ca in solution adsorbed), even in natural environments. By assuming that our results can be transposed to other phyllosilicate minerals, it is thus possible to qualitatively determine which types of minerals will potentially generate a Ca isotopic fractionation during adsorption occurring in similar conditions to those used in our experiments. According to Guggenheim et al. (2006), phyllosilicate minerals are divided into nine large groups that present different crystallographic characteristics (Table 5).

In our experimental conditions, Ca isotopic fractionation intensity is mainly related to the layer charge and, to a lesser extent, the presence of an interlayer space open to hydrated cations adsorption (at least initially in experiments). Serpentine-kaolin and talc-pyrophyllite mineral groups, which have no layer charge and no interlayer space open to hydrated cation adsorption, are thus not expected to generate a Ca isotopic fractionation during the adsorption phenomenon. Smectite and vermiculite mineral groups have an intermediate layer charge and an interlayer space open to hydrated cation adsorption. These minerals should thus generate Ca isotopic fractionation, as observed in Swy-2 adsorption experiments. For the chlorite and "variable" groups (see Table 5), estimations are difficult due to their high variability of crystallographic characteristics. The three mica groups (i.e., true, interlayer-deficient and brittle; see Table 5) should generate the highest Ca isotopic fractionation due to their very high layer charge. According to our results, this behavior could be enhanced in the case of size reduction (increased specific surface area).

If a high amount of Ca is adsorbed on these minerals and that desorption is total (by exchange with other cations located in the soil solution), none of these minerals should generate an isotopic fractionation during desorption, which was observed in our study

($\Delta^{44/40}Ca_{DES} = \Delta^{44/40}Ca_{IS}$). This observation might be explained by the proportion of adsorbed Ca relative to the Ca amount in the initial solution. Following the mass balance equation described in section 3.1., $\Delta^{44/40}Ca_{DES}$ of desorbed Ca can be calculated by:

$$\Delta^{44/40}Ca_{DES} = \frac{\left(\Delta^{44/40}Ca_{SI}\right) - \left(\Delta^{44/40}Ca_{MAA} \times (1-p)\right)}{p} \qquad (8)$$

where $\Delta^{44/40}Ca_{IS}$, $\Delta^{44/40}Ca_{DES}$ and $\Delta^{44/40}Ca_{MAA}$ represent the isotopic signatures of the initial solution, the desorbed Ca and the supernatant measured after adsorption experiments, respectively.

This calculation has been performed for different values of *p* (from 0.05 to 1); different values of $\Delta^{44/40}Ca_{MAA}$ [0.24‰, 0.10‰ and 0‰ for Tuftane muscovite (0.1-1 µm), Swy-2 and KGa-2/Tuftane muscovite (50-200 µm), respectively], corresponding to isotopic signatures measured at the isotopic steady-state of each adsorption experiment; and a constant value of $\Delta^{44/40}Ca_{IS}$ (0‰). Our results (Fig. 9) show that if we keep similar isotopic values for $\Delta^{44/40}Ca_{IS}$ and $\Delta^{44/40}Ca_{MAA}$, the amount of adsorbed Ca is a critical parameter. The amount of adsorbed Ca can change the $\Delta^{44/40}Ca_{DES}$ from 0‰ to -4.57‰ and from 0‰ to -1.80‰ for Tuftane muscovite (0.1-1 µm) and Swy-2, respectively. These values correspond to Ca adsorptions of 100% and 5%, respectively.

In our experiments, a very large amount of adsorbed Ca associated with a low intensity isotopic fractionation recorded do not allow us to record isotopic fractionation after desorption experiments ($\Delta^{44/40}Ca_{DES}$ and $\Delta^{44/40}Ca_{IS}$ are similar). Thus, for Tuftane muscovite (0.1-1 µm) and Swy-2 experiments in which an increase of $\Delta^{44/40}Ca_{MAA}$ is measured and 65% to 93% of initial Ca is adsorbed, $\Delta^{44/40}Ca_{DES}$ should be between -0.11‰ and 0‰ if desorption is total (see Fig. 9). Only adsorption of a small Ca amount associated with an important isotopic signature modification of the supernatant after adsorption experiments might generate

an important Ca isotopic fractionation during total desorption experiments. Partial desorption could generate and isotopic fractionation, as suggested by Ockert et al. (2013), and should be strongly dependent on the $\alpha_{IS\text{-}MAA}$ values, and then of the mineral and physicochemical conditions considered (see Fig. 7). This could be occurred in natural environments where it is highly unlikely to generate a total desorption, especially for minerals having an important CEC and/or layer charge. These authors also recorded Ca isotopic fractionations during adsorption on clay minerals in an oceanic context (especially on kaolinite), which were of higher intensity than those measured in the present study. Mechanisms involved to explain such a difference remain unknown, but they could be related to the different experimental conditions (e.g., solid/solution ratio, presence of NH_4^+, and ionic strength) or the use of artificial seawater as the initial solution. This rich Cl^- solution leads to particular Ca aqueous speciation {i.e., $[Ca(H_2O)_n]^{2+}$ and $[CaCl(H_2O)_n]^+$, where n is the coordination number} which can have an impact on the isotopic fractionation during Ca adsorption. Recent studies, using *ab initio* calculations, showed that significant Ca isotopic fractionation exists during fluid-mineral interactions between different species and even between the same species having different coordination numbers (Colla et al., 2013; Moynier and Fujii, 2017). For example, a Ca isotopic fractionation of 0.17‰ to 2.05‰ could exist between $CaCl(H_2O)_5^+$ and $Ca(H_2O)_n^{2+}$, depending on the coordination number (i.e., n= 6 to 8; Moynier and Fujii, 2017). None of these effects have been highlighted in our study, but more complex patterns, as in the natural environment, could potentially lead to this type of phenomena.

4. CONCLUSION

In this study, we have experimentally determined, in a batch system, that the intensity of Ca isotopic fractionations occurring during adsorption phenomena on three

phyllosilicate minerals commonly encountered within soils (a kaolinite KGa-2, a montmorillonite Swy-2 and a Tuftane muscovite with two different grain size fractions) is controlled by layer charge, the specific surface area and the interlayer space open to aqueous cation adsorption. No isotopic fractionation was recorded during KGa-2 (0.1-1 µm) and Tuftane muscovite (50-200 µm) experiments, while the light Ca isotopes (e.g., ^{40}Ca) were preferentially adsorbed on Swy-2 (0.1-1 µm) and Tuftane muscovite (0.1-1 µm). An isotopic fractionation that follows a close system equilibrium law was recorded for Tuftane muscovite (0.1-1 µm) experiments and for Swy-2 (0.1-1 µm) experiments after 65 min. For Tuftane muscovite (0.1-1 µm), this behaviour has been linked with the presence and intensity of mineral layer charge. A more complex pattern has been described for Swy-2 (0.1-1 µm), involving: (1) a kinetic isotopic fractionation generated by a selective adsorption of light isotopes (e.g., ^{40}Ca) in the interlayer space during the first time of experiments, followed by (2) an equilibration of the interlayer space with the surrounding solution, leading to a decrease of the supernatant isotopic signature, and (3) an equilibrium fractionation again linked to the intensity of the layer charge. No isotopic fractionation has been recorded during complete desorption in our conditions.

If we now transpose these results to the natural environment, we can expect that the mica group and the Smectite-Vermiculite group should generate a significant Ca isotopic fractionation during adsorption phenomena. Thus, adsorption on phyllosilicate minerals could be a non-negligible contributor to the Ca isotopic signature of the rivers.

ACKNOWLEDGMENTS

We want to thank Amélie Aubert and Gilles Morvan (LHyGeS, Strasbourg) for XRD and SEM analysis, respectively, and Jean-Dominique Comparot (IC2MP, Poitiers) for BET

741 measurements. Colin Fourtet, Thierry Perrone and René Boutin (LHyGeS, Strasbourg) are
742 acknowledged for their technical assistance in the laboratory. Valentin Robin and Damien
743 Lemarchand are thanked for helpful discussions. The manuscript benefitted from constructive
744 reviews by Edward Tipper and two anonymous reviewers. We also thank the editor, Fang-
745 Zhen Teng, for editorial handling, as well as the executive editor, Marc Norman. This project
746 was financially supported by funding from the French CNRS-INSU programme "EC2CO-
747 BIOHEFECT".

748

749 APPENDIX A. SUPPLEMENTARY MATERIAL

750

751 Supplementary data associated with this article can be found, in the online version, at
752 https://...

753

754 REFERENCES

755

756 Altman, D. G., & Bland, J. M. (2005). Standard deviations and standard errors. *Bmj*,
757 *331*(7521), 903.

758 Bagard M-L, Chabaux F, Pokrovsky O. S., Viers J., Prokushkin A. S., Stille P., Rihs S.,
759 Schmitt A.-D., Dupré B. (2011). Seasonal variability of element fluxes in two Central
760 Siberian rivers draining high latitude permafrost dominated areas Geochimica et
761 Cosmochimica Acta, 75, 3335-3357.

762 Bergaya, F., Lagaly, G., (2006). Chapter 1 General Introduction: Clays, Clay Minerals, and
763 Clay Science, in: Bergaya, F., Theng, B.K.G., Lagaly, G. (Eds.), Developments in
764 Clay Science, *Handbook of Clay Science. Elsevier*, pp. 1–18.

765 Berner, E. K., & Berner, R. A. (2012). *Global environment: water, air, and geochemical*
766 *cycles*. Princeton University Press.
767 Borchardt, G. (1989). Smectites. *Minerals in soil environments*, 675-727.
768 Brunauer, S., Emmett, P. H., & Teller, E. (1938). Adsorption of gases in multimolecular
769 layers. *Journal of the American chemical society*, ***60***, 309-319.
770 Chabaux, F., Blaes, E., Stille, P., di Chiara Roupert, R., Pelt, E., Dosseto, A., Ma, L., Buss,
771 H.L., Brantley, S.L., (2013). Regolith formation rate from U-series nuclides:
772 Implications from the study of a spheroidal weathering profile in the Rio Icacos
773 watershed (Puerto Rico). *Geochim. Cosmochim. Acta* **100**, 73–95.
774 Chipera, S.J., Bish, D.L., (2001). Baseline Studies of the Clay Minerals Society Source Clays:
775 Powder X-Ray Diffraction Analyses. *Clays Clay Miner.* **49**, 398–409.
776 Ciesielski, H., Sterckeman, T., Santerne, M., & Willery, J. P. (1997). Determination of cation
777 exchange capacity and exchangeable cations in soils by means of cobalt hexamine
778 trichloride. Effects of experimental conditions. *Agronomie*, **17**(1), 1-7.
779 Cobert, F., Schmitt, A.D., Bourgeade, P., Labolle, F., Badot, P.M., Chabaux, F. & Stille, P.
780 (2011) Experimental identification of Ca isotopic fractionations in higher plants
781 Geochimica et Cosmochimica Acta, 75, 5467-5482.
782 Colla, C. A., Wimpenny, J., Yin, Q. Z., Rustad, J. R., & Casey, W. H. (2013). Calcium-
783 isotope fractionation between solution and solids with six, seven or eight oxygens
784 bound to Ca (II). *Geochimica et Cosmochimica Acta*, ***121***, 363-373.
785 Dixon, J. B. (1989). Kaolin and serpentine group minerals. *Minerals in soil environments*,
786 467-525.
787 Dogan, A.U., Dogan, M., Onal, M., Sarikaya, Y., Aburub, A., Wurster, D.E., 2006. Baseline
788 studies of the Clay Minerals Society source clays: specific surface area by the
789 Brunauer Emmett Teller (BET) method. *Clays Clay Miner.* **54**, 62–66.

790 Douglas, L. A. (1989). Vermiculites. *Minerals in soil environments*, 635-674.

791 Eisenhauer, A., Nägler, T.F., Stille, P., Kramers, J., Gussone, N., Bock, B., Fietzke, J.,
792 Hippler, D., Schmitt, A.-D., (2004). Proposal for International Agreement on Ca
793 Notation Resulting from Discussions at Workshops on Stable Isotope Measurements
794 Held in Davos (Goldschmidt 2002) and Nice (EGS-AGU-EUG 2003). *Geostand.*
795 *Geoanalytical Res.* **28**, 149–151.

796 Fanning, D. S., Keramidas, V. Z., & El-Desoky, M. A. (1989). Micas. *Minerals in soil*
797 *environments*, 551-634.

798 Fantle, M.S., Tipper, E.T., (2014). Calcium isotopes in the global biogeochemical Ca cycle:
799 Implications for development of a Ca isotope proxy. *Earth-Sci. Rev.* **129**, 148–177.

800 Ferris, A.P., Jepson, W.B., (1975). The exchange capacities of kaolinite and the preparation of
801 homoionic clays. *J. Colloid Interface Sci.* **51**, 245–259.

802 Guggenheim, S., & Van Groos, A. K. (2001). Baseline studies of the clay minerals society
803 source clays: thermal analysis. *Clays and Clay Minerals*, ***49*****(5)**, 433-443.

804 Guggenheim, S., Adams, J.M., Bain, D.C., Bergaya, F., Brigatti, M.F., Drits, V.A., Formoso,
805 M.L.L., Galán, E., Kogure, T., Stanjek, H., (2006). Summary of Recommendations of
806 Nomenclature Committees Relevant to Clay Mineralogy: Report of the Association
807 Internationale Pour L'etude des Argiles (aipea) Nomenclature Committee for 2006.
808 *Clays Clay Miner.* **54**, 761–772.

809 Gustafsson, J. P. (2013). Visual MINTEQ version 3.1, department of sustainable
810 development. *Environmental Science and Engineering, KTH, Stockholm.*

811 Gussone, N., Dietzel, M., (2016). Calcium Isotope Fractionation During Mineral Precipitation
812 from Aqueous Solution, in: Calcium Stable Isotope Geochemistry, Advances in
813 Isotope Geochemistry. *Springer, Berlin, Heidelberg*, pp. 75–110.

814 Hakem, N., Al Mahamid, I., Apps, J., Moridis, G., (2000). Sorption of Cesium and Strontium
815 on Hanford Soil. *J. Radioanal. Nucl. Chem.* **246**, 275–278.
816 Heuser, A., Schmitt, A.-D., Gussone, N., Wombacher, F., (2016). Analytical Methods, in:
817 Calcium Stable Isotope Geochemistry, Advances in Isotope Geochemistry. *Springer,*
818 *Berlin, Heidelberg*, pp. 23–73.
819 Hindshaw, R. S., Reynolds, B. C., Wiederhold, J. G., Kiczka, M., Kretzschmar, R., &
820 Bourdon, B. (2013). Calcium isotope fractionation in alpine plants. *Biogeochemistry*,
821 ***112*(1-3)**, 373-388.
822 Hippler, D., Schmitt, A.-D., Gussone, N., Heuser, A., Stille, P., Eisenhauer, A., Nägler, T.F.,
823 (2003). Calcium Isotopic Composition of Various Reference Materials and Seawater.
824 *Geostand. Newsl.* **27**, 13–19.
825 Holmden, C. (2005). Measurement of! 44Ca Using a 43Ca-42Ca Double-spike TIMS
826 Technique.
827 Holmden, C., & Bélanger, N. (2010). Ca isotope cycling in a forested ecosystem. *Geochimica*
828 *et Cosmochimica Acta*, ***74*(3)**, 995-1015.
829 Horwitz, E.P., McAlister, D.R., Bond, A.H., Jr, R.E.B., (2005). Novel Extraction of
830 Chromatographic Resins Based on Tetraalkyldiglycolamides: Characterization and
831 Potential Applications. *Solvent Extr. Ion Exch.* **23**, 319–344.
832 Jackson, M. L. (1959). Frequency distribution of clay minerals in major great soil groups as
833 related to the factors of soil formation. *Clays and Clay Minerals*, **6**, 133-143.
834 Jackson, M. L. (1963). Interlayering of expansible layer silicates in soils by chemical
835 weathering. *Clays and Clay Minerals*, **11**, 29-46.
836 Levy, R., & Shainberg, I. (1972). Calcium-magnesium exchange in montmorillonite and
837 vermiculite. *Clays Clay Miner*, **20**, 37-46.

838 Li, D., Liu, S.-A., Li, S., (2015). Copper isotope fractionation during adsorption onto
839 kaolinite: Experimental approach and applications. *Chem. Geol.* **396**, 74–82.
840 Liu, D.-C., Hsu, C.-N., Chuang, C.-L., (1995). Ion-exchange and sorption kinetics of cesium
841 and strontium in soils. *Appl. Radiat. Isot.* **46**, 839–846.
842 Lu, J., Tertre, E., Beaucaire, C., (2014). Assessment of a predictive model to describe the
843 migration of major inorganic cations in a Bt soil horizon. *Appl. Geochem.* **41**, 151–
844 162.
845 Ma, C., Eggleton, R.A., (1999). Cation exchange capacity of kaolinite. *Clays Clay Miner.* **47**,
846 174–180.
847 Madejova, J., & Komadel, P. (2001). Baseline studies of the clay minerals society source
848 clays: infrared methods. *Clays and clay minerals*, ***49*****(5)**, 410-432.
849 Marschner H. (1995) Mineral nutrition of higher plants (second edition). *Academic Press,*
850 *London*, 889p.
851 McBride, M.B., (1994). Environmental chemistry of soils. *Environ. Chem. Soils.*
852 McCauley, A., Jones, C., & Jacobsen, J. (2009). Soil pH and organic matter. *Nutrient*
853 *management module*, **8**, 1-12.
854 Mckenzie, R. C., & Milne, A. A. (1953). The effect of grinding on micas, I. Muscovite.
855 *Mineral. Mag*, **30**, 178-185.
856 Mermut, A. R., & Cano, A. F. (2001). Baseline studies of the clay minerals society source
857 clays: chemical analyses of major elements. *Clays and Clay Minerals*, ***49*****(5)**, 381-386.
858 Mermut, A. R., & Lagaly, G. (2001). Baseline studies of the clay minerals society source
859 clays: layer-charge determination and characteristics of those minerals containing 2: 1
860 layers. *Clays and Clay Minerals*, **49(5)**, 393-397.
861 Meunier, A. (2005). *Clays. Springer Science & Business Media.*

862 Meybeck, M., (1987). Global chemical weathering of surficial rocks estimated from river
863 dissolved loads. *Am. J. Sci.* **287**, 401–428.
864 Millot, R., & Girard, J. P. (2007). Lithium isotope fractionation during adsorption onto
865 mineral surfaces. In *International Meeting on Clays in Natural & Engineered Barriers*
866 *for Radioactive Waste Confinement*, Lille, France.
867 Missana, T., Garcia-Gutierrez, M., Alonso, U., (2008). Sorption of strontium onto
868 illite/smectite mixed clays. Phys. Chem. Earth Parts ABC, *Clays in Natural &*
869 *Engineered Barriers for Radioactive Waste Confinement* **33**, S156–S162.
870 Mitchell, J. K., & Soga, K. (2005). Fundamentals of soil behavior.
871 Moore, D. M., & Reynolds, R. C. (1989). X-ray Diffraction and the Identification and
872 Analysis of Clay Minerals (Vol. **378**, p. 155). *Oxford: Oxford university press.*
873 Moll, W.F., (2001). Baseline Studies of the Clay Minerals Society Source Clays: Geological
874 Origin. *Clays Clay Miner.* **49**, 374–380.
875 Moynier, F., & Fujii, T. (2017). Calcium isotope fractionation between aqueous compounds
876 relevant to low-temperature geochemistry, biology and medicine. *Scientific Reports*, **7**.
877 Ockert, C., Gussone, N., Kaufhold, S., Teichert, B.M.A., (2013). Isotope fractionation during
878 Ca exchange on clay minerals in a marine environment. *Geochim. Cosmochim. Acta*
879 **112**, 374–388.
880 Oelkers, E. H., Schott, J., & Devidal, J. L. (1994). The effect of aluminum, pH, and chemical
881 affinity on the rates of aluminosilicate dissolution reactions. *Geochimica et*
882 *Cosmochimica Acta*, *58*(9), 2011-2024.
883 Osman, M. A., & Suter, U. W. (2000). Determination of the cation-exchange capacity of
884 muscovite mica. *Journal of colloid and interface science*, **224**, 112-115.

885 Papirer, E., Roland, P., Nardin, M., Balard, H., (1986). Variation of the surface energy
886 characteristics of mica (muscovite) upon grinding. *J. Colloid Interface Sci.* **113**, 62–
887 66.
888 Párez-Maqueda, L.A., Franco, F., Avilés, M.A., Poyato, J., Pérez-Rodríguez, J.L., (2003).
889 Effect of Sonication on Particle-size Distribution in Natural Muscovite and Biotite.
890 *Clays Clay Miner.* **51**, 701–708.
891 Pelt, E., Chabaux, F., Stille, P., Innocent, C., Ghaleb, B., Girard, M., Guntzer, F. (2013)
892 Atmospheric dust contribution to the budget of U-series nuclides in soils from the
893 Mount Cameroon volcano, Chemical Geology, **341**, 147-157.
894 Reinholdt, M. X., Hubert, F., Faurel, M., Tertre, E., Razafitianamaharavo, A., Francius, G.,
895 Prêt, D., Petit, S., Béré, E., Pelletier, M., Ferrage, E. (2013). Morphological properties
896 of vermiculite particles in size-selected fractions obtained by sonication. *Applied Clay*
897 *Science*, ***77***, 18-32.
898 Robin, V., Tertre, E., Beaufort, D., Regnault, O., Sardini, P., Descostes, M., (2015). Ion
899 exchange reactions of major inorganic cations (H+, Na+, Ca2+, Mg2+ and K+) on
900 beidellite: Experimental results and new thermodynamic database. Toward a better
901 prediction of contaminant mobility in natural environments. *Appl. Geochem.* **59**, 74–
902 84.
903 Romaniello, S.J., Field, M.P., Smith, H.B., Gordon, G.W., Kim, M.H., Anbar, A.D., (2015).
904 Fully automated chromatographic purification of Sr and Ca for isotopic analysis. *J.*
905 *Anal. At. Spectrom.* **30**, 1906–1912.
906 Schmitt, A.-D., Bracke, G., Stille, P., Kiefel, B., (2001). The Calcium Isotope Composition of
907 Modern Seawater Determined by Thermal Ionisation Mass Spectrometry. *Geostand.*
908 *Newsl.* **25**, 267–275.

Schmitt, A.-D., Chabaux, F., Stille, P., (2003). The calcium riverine and hydrothermal isotopic fluxes and the oceanic calcium mass balance. *Earth Planet. Sci. Lett.* **213**, 503–518.

Schmitt, A.-D., Gangloff, S., Cobert, F., Lemarchand, D., Stille, P., Chabaux, F., (2009). High performance automated ion chromatography separation for Ca isotope measurements in geological and biological samples. *J. Anal. At. Spectrom.* **24**, 1089–1097.

Schmitt, A.-D., Cobert, F., Bourgeade, P., Ertlen, D., Labolle, F., Gangloff, S., Badot, P.-M., Chabaux, F., Stille, P., (2013). Calcium isotope fractionation during plant growth under a limited nutrient supply. *Geochim. Cosmochim. Acta* **110**, 70–83.

Schmitt A. D. (2016) Earth-surface Ca isotopic fractionations. In: Gussone N., Schmitt A.-D., Heuser A., Wombacher F., Dietzel M., Tipper E., Schiller M. "Calcium Stable Isotope Geochemistry", *Springer*, pp 145-172.

Schmitt, A. D., Gangloff, S., Labolle, F., Chabaux, F., & Stille, P. (2017). Calcium biogeochemical cycle at the beech tree-soil solution interface from the Strengbach CZO (NE France): insights from stable Ca and radiogenic Sr isotopes. *Geochimica et Cosmochimica Acta*, ***213***, 91-109.

Schmitt, A. D., Borrelli, N., Ertlen, D., Gangloff, S., Chabaux, F., & Osterrieth, M. (2018). Stable calcium isotope speciation and calcium oxalate production within beech tree (Fagus sylvatica L.) organs. *Biogeochemistry*, ***137*****(1-2)**, 197-217.

Schroth, B.K., Sposito, G., (1997). Surface Charge Properties of Kaolinite. *MRS Online Proc. Libr. Arch.* **432**.

Sivamohan, R., Vachot, P., (1990). A comparative study of stirred and vibratory mills for the fine grinding of muscovite, wollastonite and kaolinite. *Powder Technol.* **61**, 119–129.

Sposito, G., Holtzclaw, K.M., Jouany, C., Charlet, L., (1983). Cation Selectivity in Sodium-Calcium, Sodium-Magnesium, and Calcium-Magnesium Exchange on Wyoming Bentonite at 298 K. *Soil Sci. Soc. Am. J.* **47**, 917–921.

Sposito, G., Skipper, N.T., Sutton, R., Park, S., Soper, A.K., Greathouse, J.A., (1999). Surface geochemistry of the clay minerals. *Proc. Natl. Acad. Sci.* **96**, 3358–3364. doi:10.1073/pnas.96.7.3358

Stille, P, Schmitt, AD, Labolle, F, Pierret, MC, Gangloff, S, Cobert, F, Lucot, E, Gueguen, F, Brioschi, L, Steinmann, M & Chabaux, F (2012). The suitability of annual tree growth rings as environmental archives: Evidence from Sr, Nd, Pb and Ca isotopes in spruce growth rings from the Strengbach watershed CR Geoscience, 344, 297-311.

Taiz L., Zeiger E. (2010) Plant Physiology, Fifth edition. *Sinauer Associates Inc*., 782pp.

Tertre, E., Castet, S., Berger, G., Loubet, M., & Giffaut, E. (2006). Surface chemistry of kaolinite and Na-montmorillonite in aqueous electrolyte solutions at 25 and 60 C: experimental and modeling study. *Geochimica et Cosmochimica Acta, **70***, 4579-4599.

Tertre, E., Ferrage, E., Bihannic, I., Michot, L.J., Prêt, D., (2011a). Influence of the ionic strength and solid/solution ratio on Ca(II)-for-Na+ exchange on montmorillonite. Part 2: Understanding the effect of the m/V ratio. Implications for pore water composition and element transport in natural media. *J. Colloid Interface Sci.* **363**, 334–347.

Tertre, E., Prêt, D., Ferrage, E., (2011b). Influence of the ionic strength and solid/solution ratio on Ca(II)-for-Na+ exchange on montmorillonite. Part 1: Chemical measurements, thermodynamic modeling and potential implications for trace elements geochemistry. *J. Colloid Interface Sci.* **353**, 248–256.

Tertre, E., Hubert, F., Bruzac, S., Pacreau, M., Ferrage, E., Prêt, D., (2013). Ion-exchange reactions on clay minerals coupled with advection/dispersion processes. Application to

Na+/Ca2+ exchange on vermiculite: Reactive-transport modeling, batch and stirred flow-through reactor experiments. *Geochim. Cosmochim. Acta* **112**, 1–19.

Tertre, E., Delville, A., Prêt, D., Hubert, F., & Ferrage, E. (2015). Cation diffusion in the interlayer space of swelling clay minerals–A combined macroscopic and microscopic study. *Geochimica et Cosmochimica Acta*, ***149***, 251-267.

Thomas, G.W., (1996). Soil pH and Soil Acidity. Methods Soil Anal. Part 3—*Chemical Methods*, 475–490.

Tipper, E.T., Gaillardet, J., Galy, A., Louvat, P., Bickle, M.J., Capmas, F., (2010). Calcium isotope ratios in the world's largest rivers: A constraint on the maximum imbalance of oceanic calcium fluxes. *Glob. Biogeochem. Cycles* **24**, GB3019.

Tipper E. T., Schmitt A. D. and Gussone N. (2016) Global Ca cycles: coupling of continental and oceanic processes. In: Gussone N., Schmitt A.-D., Heuser A., Wombacher F., Dietzel M., Tipper E., Schiller M. "Calcium Stable Isotope Geochemistry", *Springer*,173-222.

Tournassat, C., Greneche, J.-M., Tisserand, D., Charlet, L., (2004a). The titration of clay minerals: I. Discontinuous backtitration technique combined with CEC measurements. *J. Colloid Interface Sci.* **273**, 224–233.

Tournassat, C., Ferrage, E., Poinsignon, C., Charlet, L., (2004b). The titration of clay minerals: II. Structure-based model and implications for clay reactivity. *J. Colloid Interface Sci.* **273**, 234–246.

Tournassat, C., Gailhanou, H., Crouzet, C., Braibant, G., Gautier, A., Gaucher, E.C., (2009). Cation Exchange Selectivity Coefficient Values on Smectite and Mixed-Layer Illite/Smectite Minerals. *Soil Sci. Soc. Am. J.* **73**, 928–942.

Vogt, C., Lauterjung, J., Fischer, R.X., (2002). Investigation of the Clay Fraction (<2 μm) of the Clay Minerals Society Reference Clays. *Clays Clay Miner*. **50**, 388–400.

Wahlberg, J. S., Baker, J. H., Vernon, R. W., & Dewar, R. S. (1965). Exchange adsorption of strontium on clay minerals (No. 1140-C). US Govt. Print. Off.,.

Walker, J.C.G., Hays, P.B., Kasting, J.F., (1981). A negative feedback mechanism for the long-term stabilization of Earth's surface temperature. *J. Geophys. Res. Oceans* **86**, 9776–9782.

Weil, R. R., & Brady, N. C., (2017). The Nature and Properties of Soil, Fifteenth edition. *Pearson education.*

Wilson, M. J. (1999). The origin and formation of clay minerals in soils: past, present and future perspectives. *Clay Minerals, **34**,* 7-25.

Figure Captions

Figure 1. *Ca separation experiments on TODGA resin. An artificial solution containing 50 µg of each element has been loaded on the resin.*

Figure 2. *The amount (in µmol) of Ca measured in the 40 mL supernatant recovered after the adsorption experiments and in the 20 mL supernatant recovered after the desorption. The experiments used 100 mg of each mineral and 40 mL of initial solution and were carried out at pH=4 and at pH=7 as a function of time (up to 48 h). The desorption experiment was not performed for Tuftane muscovite (50-200 µm) at pH=4 due to absence of Ca adsorption.*

Figure 3. *$\Delta^{44/40}Ca_{MAA}$ and $\Delta^{44/40}Ca_{MAD}$ calculated between the isotopic value of the initial solution and the isotopic values measured in 40 mL of supernatant recovered after the adsorption experiments (red circles) and in the 20 mL supernatant recovered after the desorption (blue square). The experiments used 100 mg of each mineral. No isotopic values*

were measured for experiments performed with Tuftane muscovite at pH=4 due to the absence of elementary Ca adsorption. $\Delta^{44/40}Ca_{DES}$ calculated following the mass balance equation in section 3.1. (Eq.4) are represented by green triangle. IS=initial solution, IP=isotopic plateau, ads=adsorption, des=desorption, meas=measured, calcul= calculated.

Figure 4. *Amount of Ca remaining in the supernatant recovered after the adsorption and desorption experiments and the apparent isotopic fractionation between the initial solution and the supernatant recovered after adsorption ($\Delta^{44/40}Ca_{MAA}$, red circle) and desorption ($\Delta^{44/40}Ca_{MAD}$, blue square) experiments. Experiments were performed by using 100 mg each of KGa-2 and Swy-2 and 40 mL of the initial solution. The data were obtained by considering: (A and B) the different fixed concentrations of Mg, Sr and K to test cationic competition and (C and D) the different fixed concentrations of NaCl to test the ionic strength effect. $\Delta^{44/40}Ca_{DES}$ calculated following the mass balance equation in section 3.1. (Eq.4) are represented by green triangle.*
IS=initial solution, ads=adsorption, des=desorption, meas=measured, calcul= calculated

Figure 5. *SEM images of Tuftane muscovite (50-200 µm) (on the left) and Tuftane muscovite (0.1-1 µm) (on the right). Delamination is predominant for the lowest size fraction.*

Figure 6. *Time to reach a chemical stationary state for the Ca adsorption reaction as a function of the cation exchange capacity (CEC) of each mineral.*

Figure 7. *Comparison between the calculated $\Delta^{44/40}Ca_{MAA}$ values, considering a closed system equilibrium fractionation law (see equation 6 in the text), with measured ones for (A and B) Swy-2 and (C and D) Tuftane muscovite (0.1-1 µm), both at pH=4 and pH=7. The three*

isotopic fractionation ratio values (i.e., α) are given by: blue values=lowest values, green values=mean values and red values= highest values.

Figure 8. *Schematic drawing of different processes occurring during Ca adsorption onto Swy-2 particles [i.e., TOT–(interlayer space)–TOT] and their effects on* $\Delta^{44/40}Ca_{MAA}$*. (A) Selective adsorption of light isotopes (e.g.,* ^{40}Ca*) in interlayer space leads to an increase of* $\Delta^{44/40}Ca_{MAA}$*. (B) Equilibration of the interlayer space with the surrounding solution leads to a decrease of* $\Delta^{44/40}Ca_{MAA}$*, and (C) selective adsorption of light isotopes (e.g.,* ^{40}Ca*) onto basal surface sites leads to an increase of* $\Delta^{44/40}Ca_{MAA}$*. (D) A synthesized conceptual illustration is presented [see text for detailed explanations of (1), (2) and (3)]. Grey tetrahedral layers, octahedral layers, or interlayer spaces, like grey isotopes, are not involved in the described reactions. IF= isotopic fractionation.*

Figure 9. *Results of* $\Delta^{44/40}Ca_{DES}$ *mass balance calculation as a function of the fraction of Ca adsorbed onto the mineral at the chemical stationary state.*

Table Captions

Table 1. *Measured cation exchange capacities (CEC), obtained from protocol of Ciesielski et al. (1997), percentages of CEC values represented by Na cations, and BET N2 specific surface areas of the phyllosilicates used. The layer charge values and the possible accessibility of the interlayer space to aqueous cations are taken from:* [1] *Schroth and Sposito (1997),* [2] *Mermut and Lagaly (2002),* [3] *Mermut and Lagaly (2002) and* [4] *Guggenheim et al. (2006).*

Table 2. *The amount of adsorbed Ca and the apparent isotopic fractionation between the initial solution and the supernatant after adsorption experiments using 100 mg of each mineral at each grain size fraction. The amount of adsorbed Ca (in µmol) is calculated from the initial amount of Ca minus the amount of Ca measured in the supernatant after adsorption experiments.* $\Delta^{44/40}Ca_{MAA}$ *1 and* $\Delta^{44/40}Ca_{MAA}$ *2 represents the first measurements and replicates, respectively while* $\Delta^{44/40}Ca_{MAAmean}$ *represents the mean values. Uncertainties on isotopic measurements have been calculated following an uncertainty propagation calculation (see Eq.3 and section 2.4. for more details). KGa-2 and Swy-2 have the same size distribution as the one for the Tuftane muscovite used (i.e., 0.1-1 µm) (see section 2.1. in the text for preparation procedure).*

IS=initial solution, MAA=measured after adsorption experiments.

Table 3. *The amount of desorbed Ca and the apparent isotopic fractionation between the initial solution and the supernatant after desorption experiments uncorrected and corrected with respect to the Ca contributions of the residual liquid and the chloride hexaamine-cobalt (HC) solution. The amounts of desorbed Ca (in µmol) in the 40 mL supernatant were measurement after desorption experiments. The contributions of Ca of the residual liquid and the HC solution are given as a percentage of the total amount of Ca measured after the desorption experiment.* $\Delta^{44/40}Ca_{MAD}$ *1 and* $\Delta^{44/40}Ca_{MAD}$ *2 represents the first measurements and the replicates, respectively while* $\Delta^{44/40}Ca_{MADmean}$ *represent the mean values. Uncertainties on isotopic measurements have been calculated following an uncertainty propagation calculation (see Eq.3 and section 2.4. for more details). KGa-2 and Swy-2 have the same size distribution as the one for the Tuftane muscovite used (i.e., 0.1-1 µm) (see section 2.1. in the text for preparation procedure).*

IS=initial solution, HC=hexaamine-cobalt, MAD= measured after desorption experiments.

Table 4. *The amount of adsorbed and desorbed Ca and the apparent isotopic fractionation between initial solution and supernatant after adsorption and desorption experiments uncorrected and corrected with respect to the Ca contributions of the residual liquid and the chloride hexaamine-cobalt (HC) solution. The amounts of adsorbed and desorbed Ca, K, Sr and Mg (in µmol) are measured in the 40 mL supernatant after adsorption and desorption experiments. The contributions of Ca of the residual liquid and the HC solution are given as a percentage of the total amount of Ca measured after the desorption experiment. Uncertainties on isotopic measurements have been calculated following an uncertainty propagation calculation (see Eq.3 and section 2.4. for more details).*

HC=hexaamine-cobalt.

Table 5. *Crystallographic characteristics of phyllosilicates commonly encountered within soils. Layer charges are given per formula unit (p.f.u.). Modified from Guggenheim et al. (2006).*

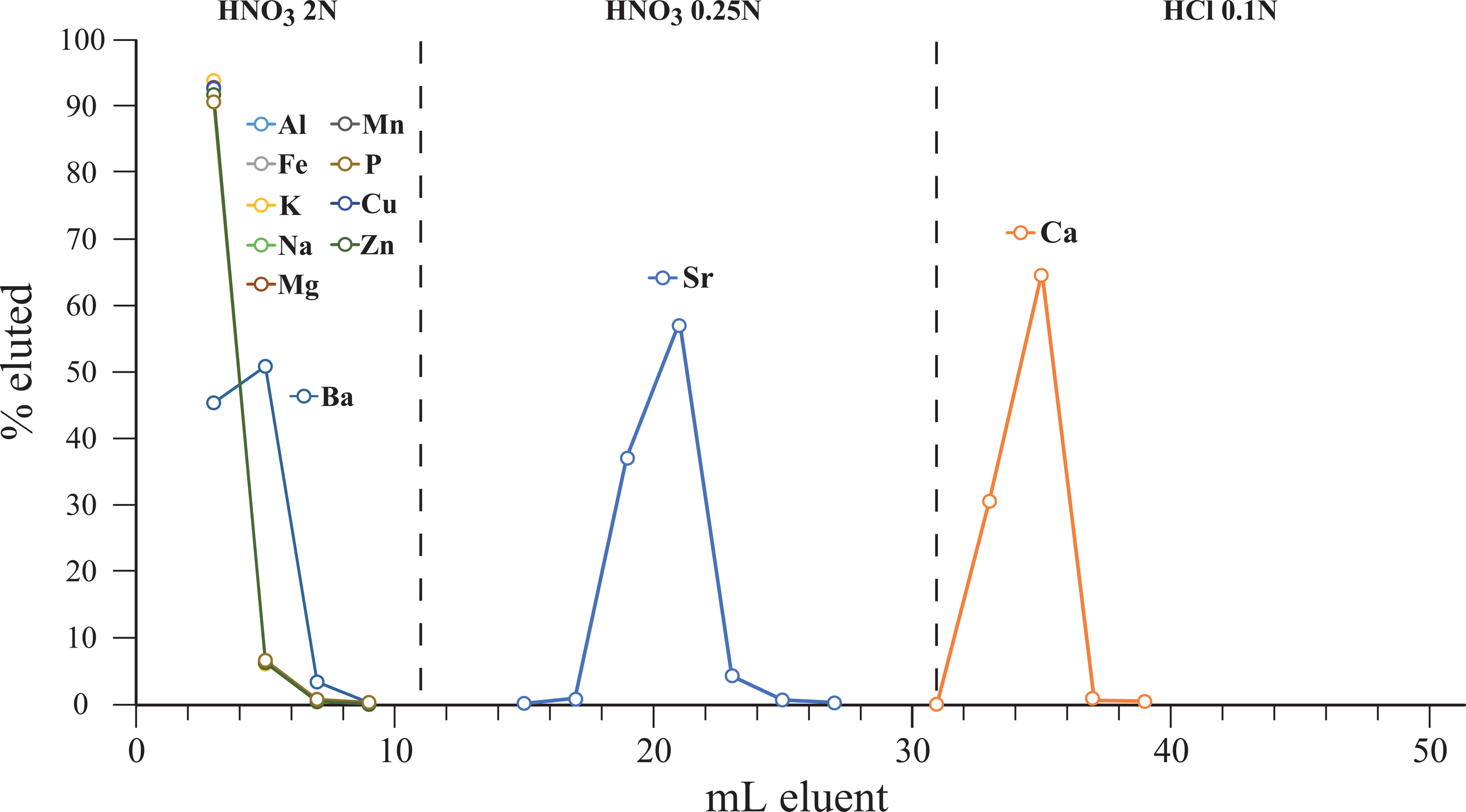
HNO3 2N
HNO3 0.25N
HCl 0.1N
Al
Mn
Fe
P
K
Cu
Na
Zn
Mg
Ba
Sr
Ca
% eluted
mL eluent
0
10
20
30
40
50
60
70
80
90
100

A KGa-2 pH=4

B KGa-2 pH=7

C Tuftane muscovite (50-200 µm) pH=4

D Tuftane muscovite (50-200 µm) pH=7

E Tuftane muscovite (0.1-1 µm) pH=4

F Tuftane muscovite (0.1-1 µm) pH=7

G Swy-2 pH=4

H Swy-2 pH=7

Ca after adsorption

Ca after desorption

Ca in the supernatant (µmol)

Time (minutes)

0 50 100 150 420 1440 2880

A KGa-2 pH=4

B KGa-2 pH=7

C Tuftane muscovite (50-200 µm) pH=4

Non measurable

D Tuftane muscovite (50-200 µm) pH=7

E Tuftane muscovite (0.1-1 µm) pH=4

F Tuftane muscovite (0.1-1 µm) pH=7

G Swy-2 pH=4

H Swy-2 pH=7

Uncertainties*

Ca after ads. meas. ($\Delta^{44/40}Ca_{MAA}$)

Ca after des. meas. ($\Delta^{44/40}Ca_{MAD}$)

Ca after des. calcul. ($\Delta^{44/40}Ca_{DES}$)

IS mean value

IS 2SE (N=16)

IP mean value

IP 2SE

$\Delta^{44/40}Ca$ (‰ SRM915a)

0.4 0.3 0.2 0.1 0 -0.1 -0.2 -0.3

0 50 100 150 420 1440 2880

Time (minutes)

A1 KGa-2 pH=7 / 125 min

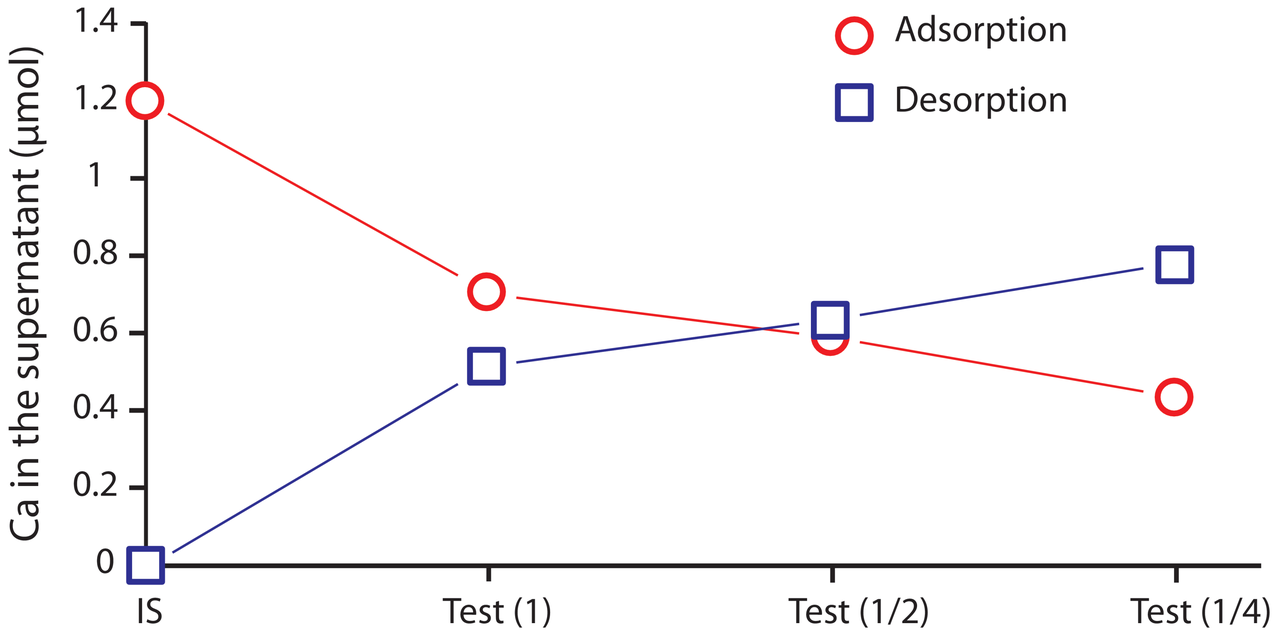

B1 Swy-2 pH=7 / 125 min

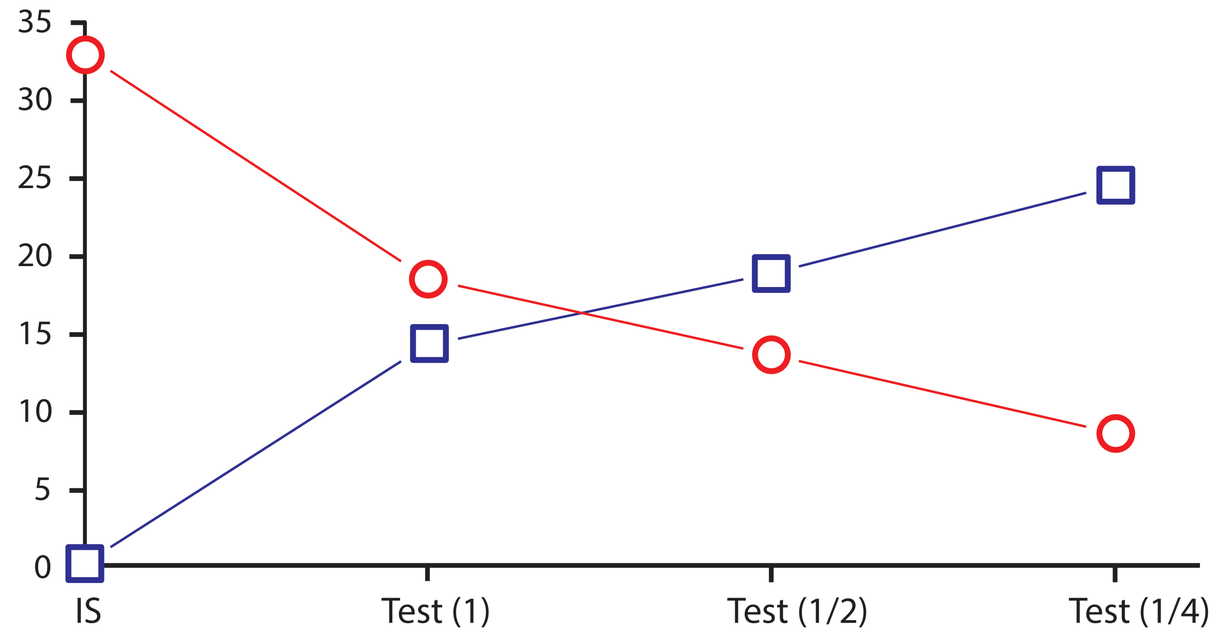

A2 KGa-2 pH=7 / 125 min

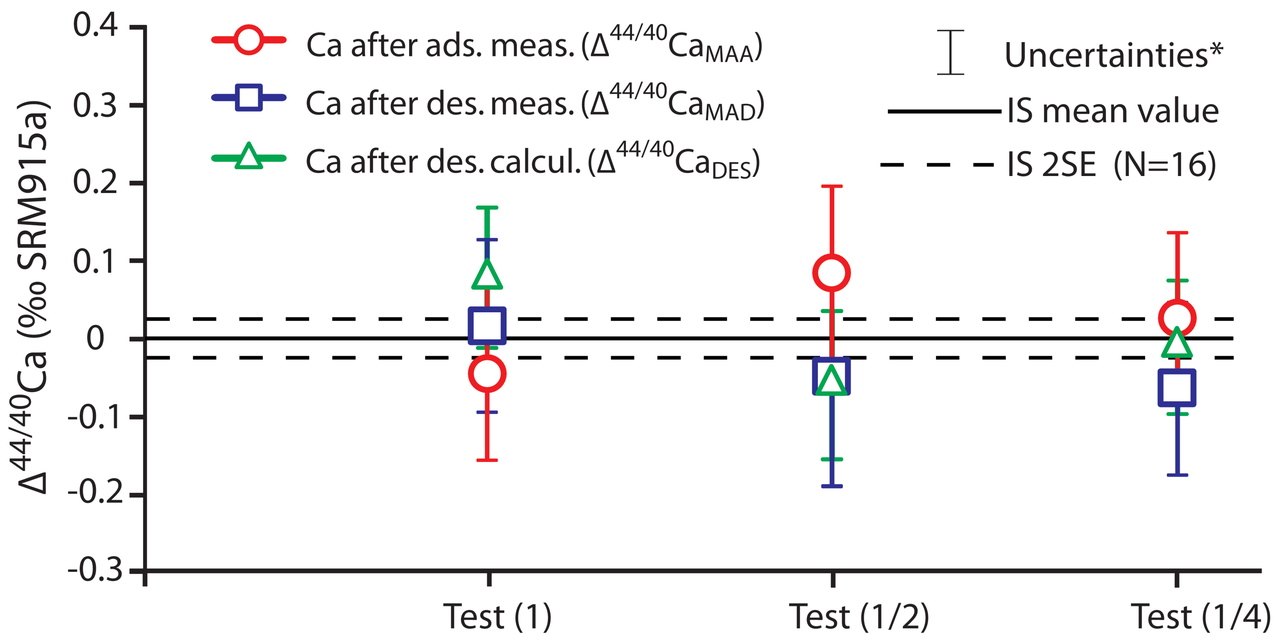

B2 Swy-2 pH=7 / 125 min

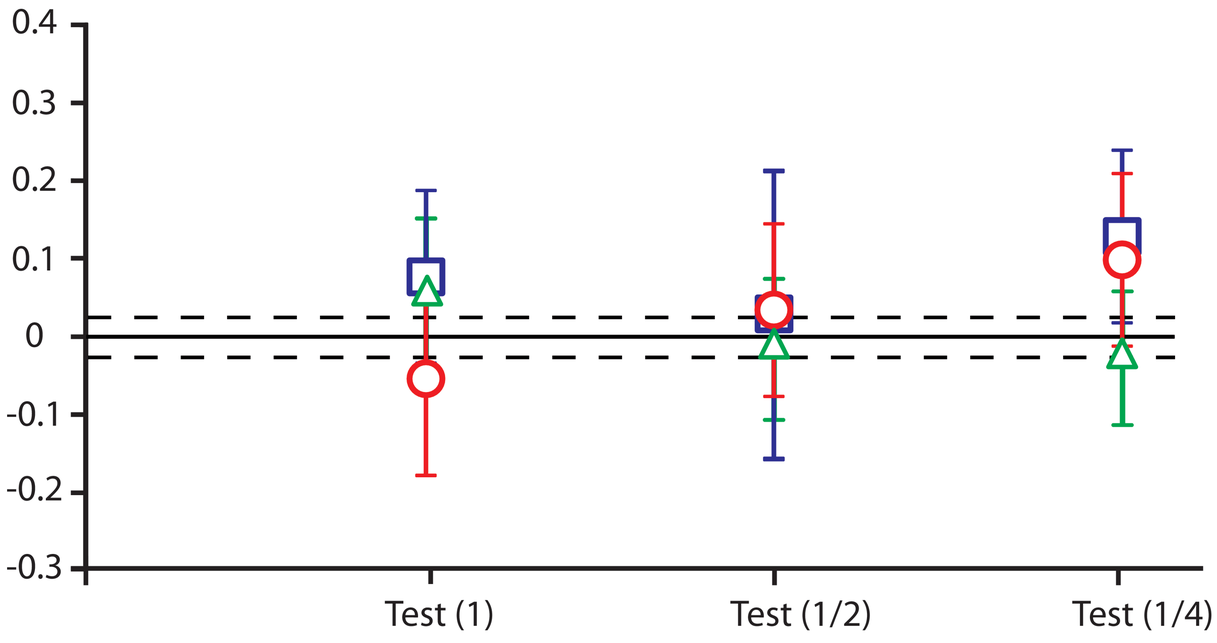

C1 KGa-2 pH=7 / 125 min

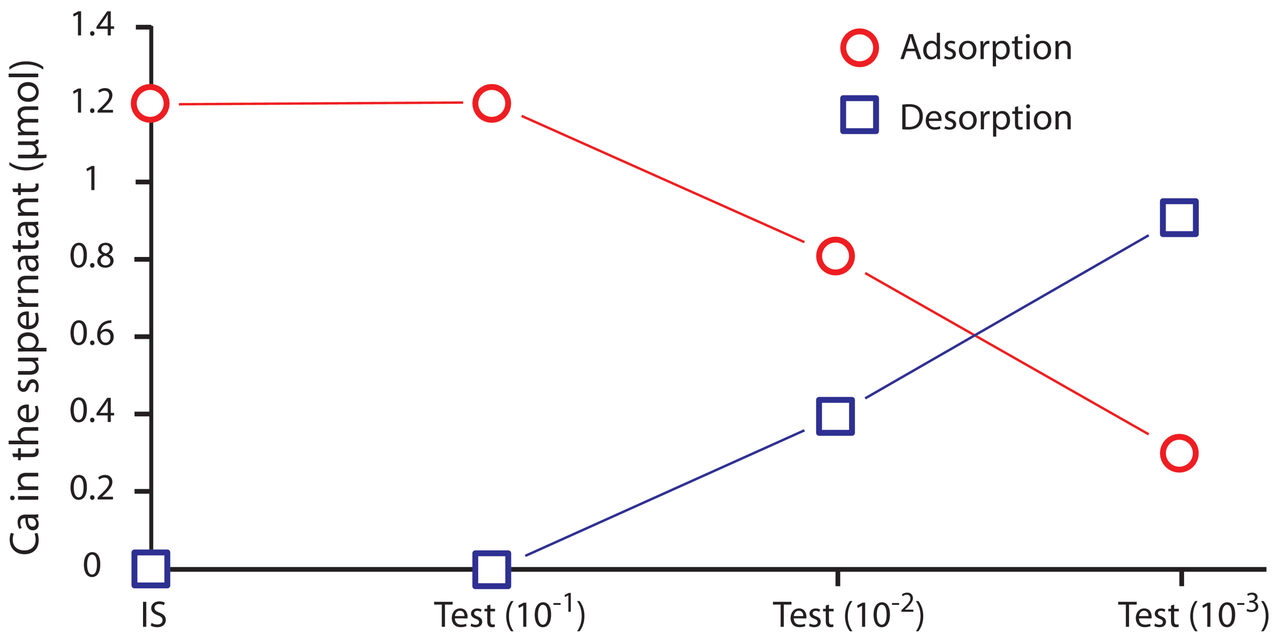

D1 Swy-2 pH=7 / 125 min

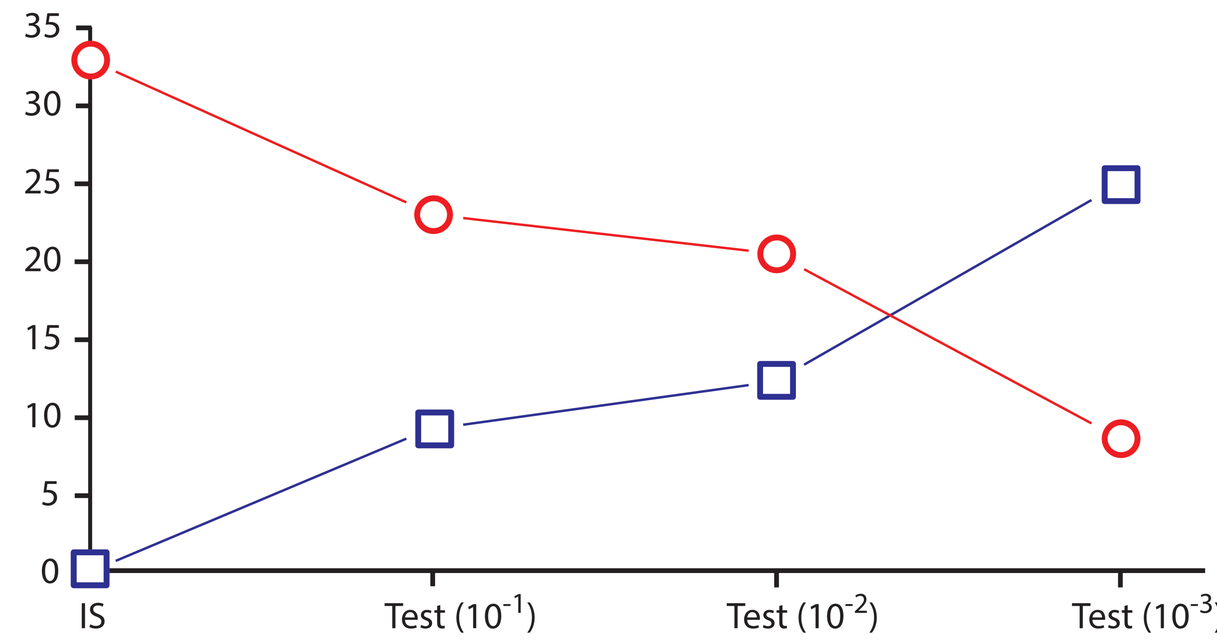

C2 KGa-2 pH=7 / 125 min

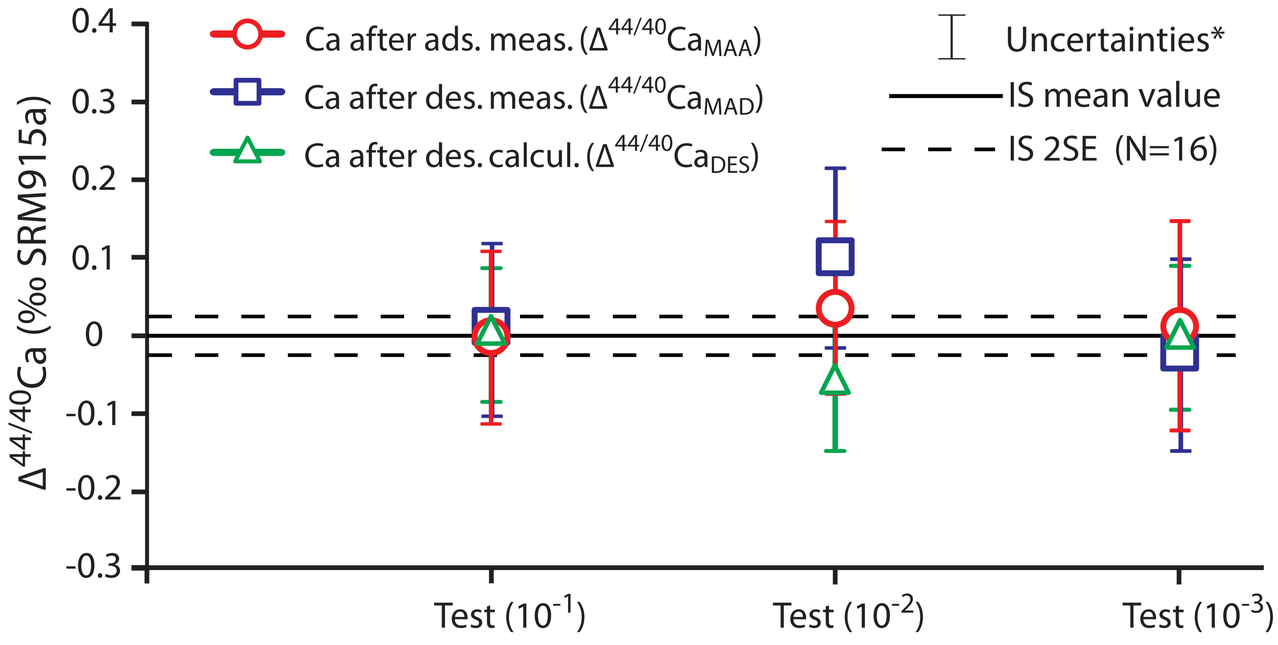

D2 Swy-2 pH=7 / 125 min

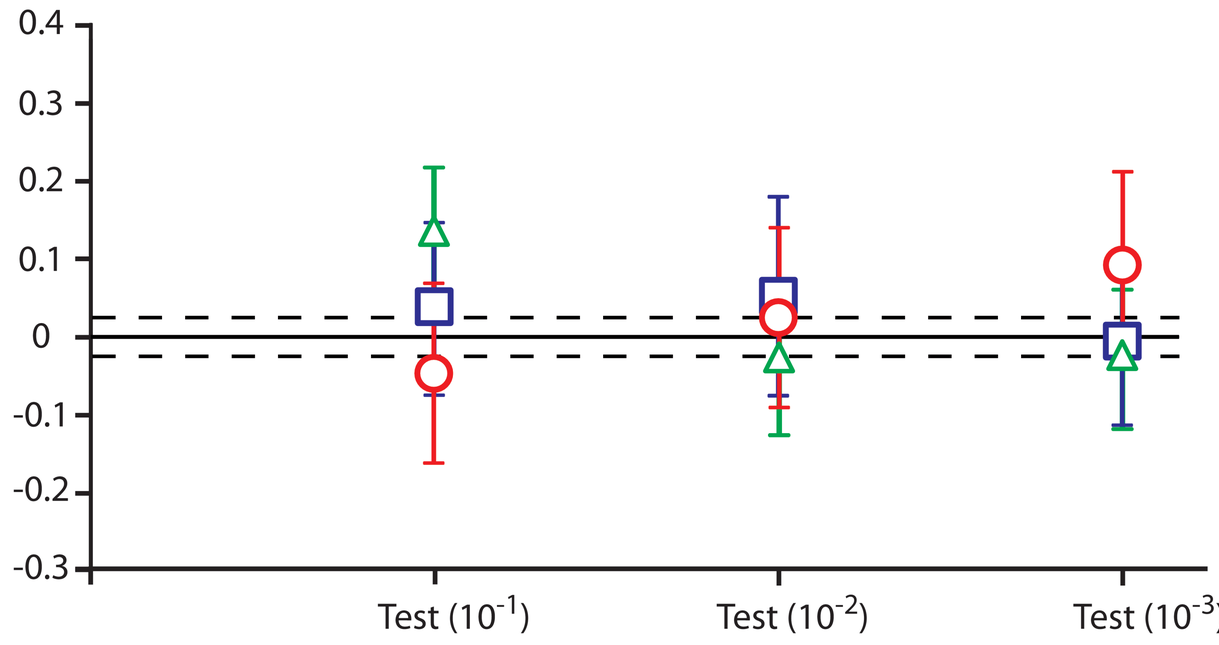

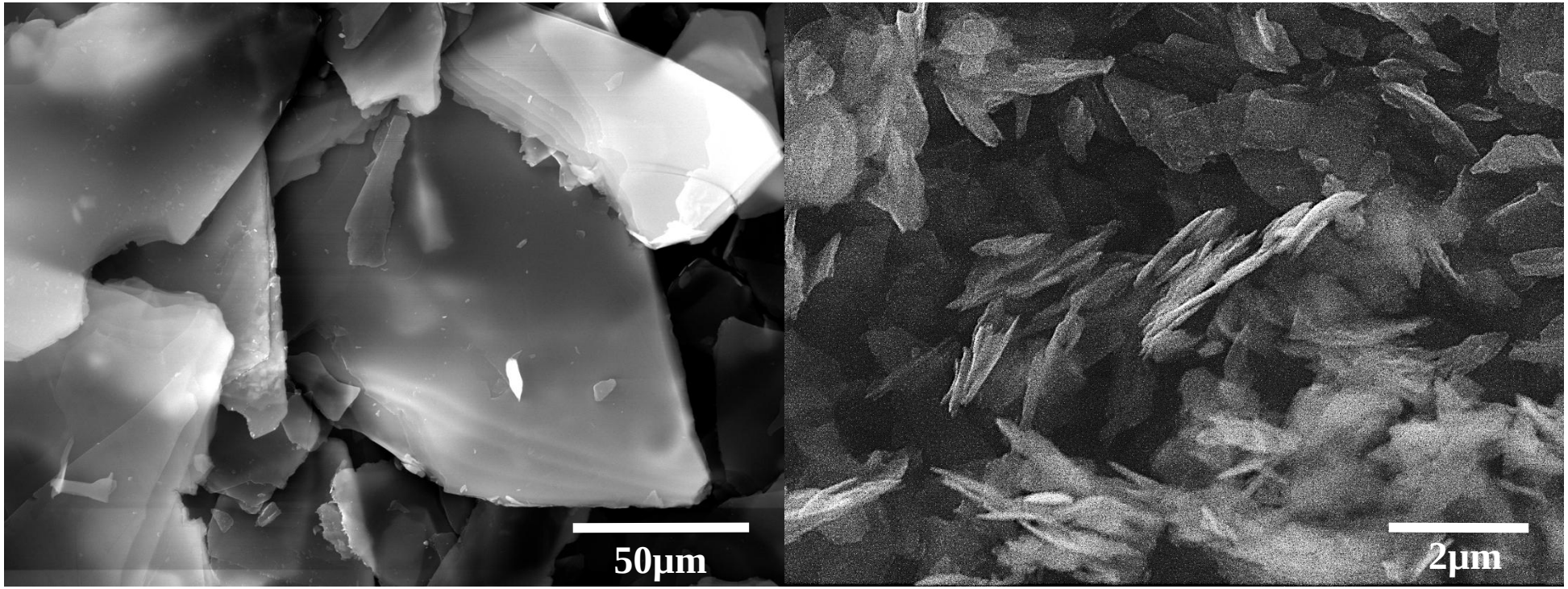
50μm
2μm

Time to reach a chemical stationary state (min)

70
60
50
40
30
20
10
0

Swy-2
(0.1-1 µm)

Tuftane muscovite
(0.1-1 µm)

$y = 9.5052 * e^{0.0247x}$
$R^2 = 0.9986$

Tuftane muscovite
(50-200 µm)

KGa-2
(0.1-1µm)

0 10 20 30 40 50 60 70 80

Cation exchange capacity (meq.100g^{-1})

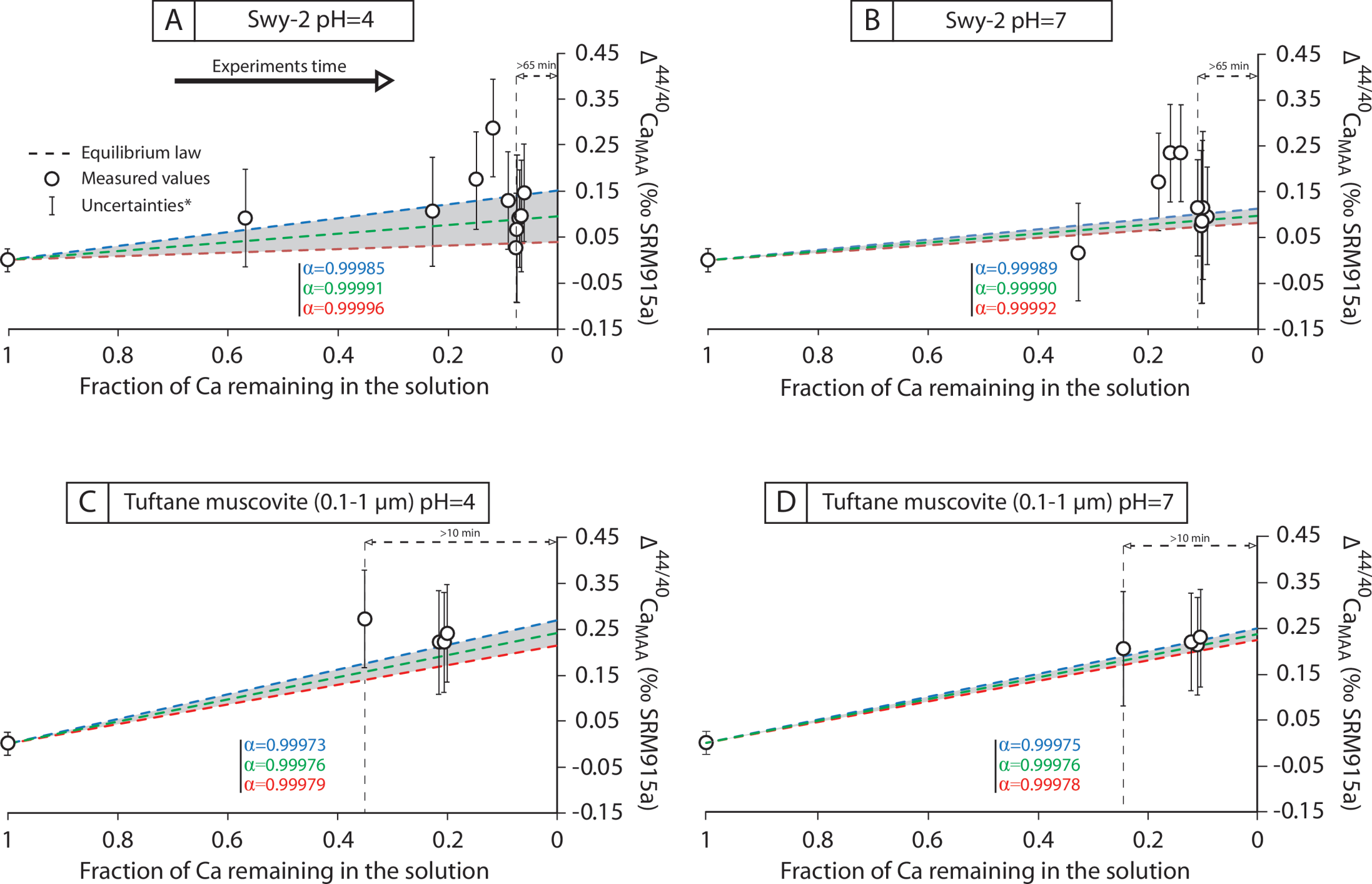
A
Swy-2 pH=4
Experiments time
>65 min
Equilibrium law
Measured values
Uncertainties*
α=0.99985
α=0.99991
α=0.99996
Δ44/40CaMAA (‰ SRM915a)
Fraction of Ca remaining in the solution
B
Swy-2 pH=7
>65 min
α=0.99989
α=0.99990
α=0.99992
Δ44/40CaMAA (‰ SRM915a)
Fraction of Ca remaining in the solution
C
Tuftane muscovite (0.1-1 µm) pH=4
>10 min
α=0.99973
α=0.99976
α=0.99979
Δ44/40CaMAA (‰ SRM915a)
Fraction of Ca remaining in the solution
D
Tuftane muscovite (0.1-1 µm) pH=7
>10 min
α=0.99975
α=0.99976
α=0.99978
Δ44/40CaMAA (‰ SRM915a)
Fraction of Ca remaining in the solution

A

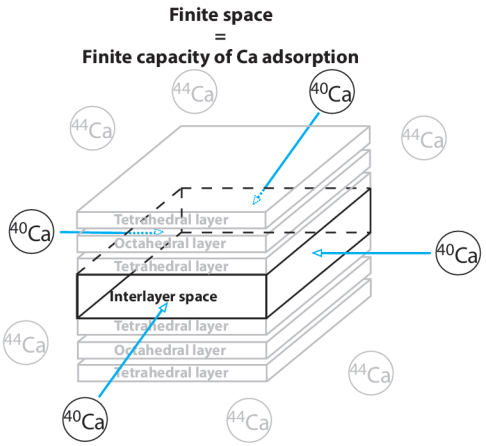

High selectivity for light isotopes (e.g., ^{40}**Ca**)

Heavy isotope (e.g., ^{44}**Ca**) **remain in solution**

Increase of solution $\delta^{44/40}$Ca signature

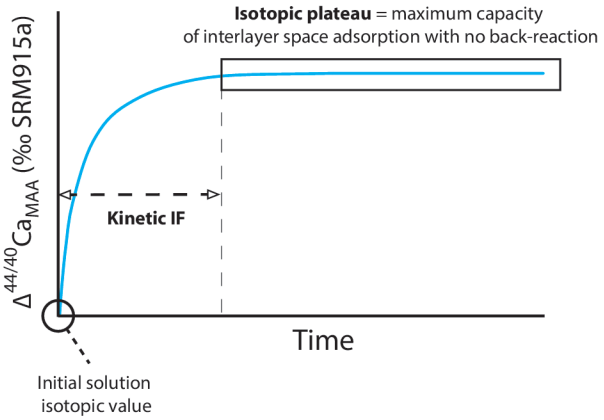

B

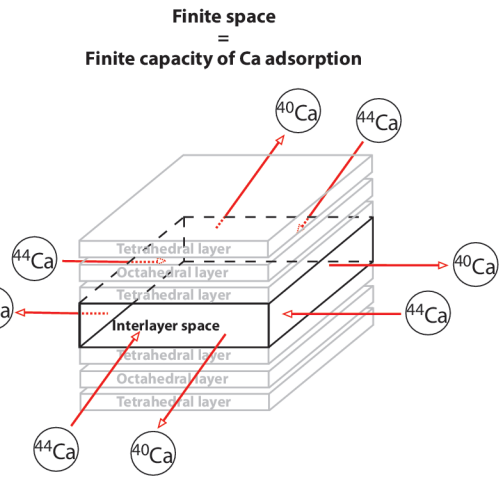

Equilibration with surrounding solution

Decrease of solution $\delta^{44/40}$Ca signature

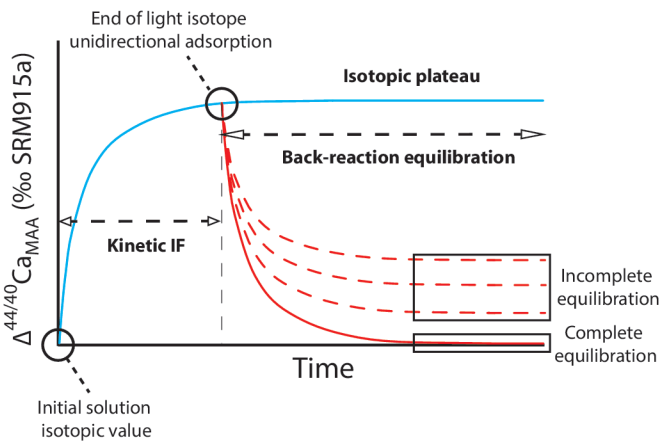

C

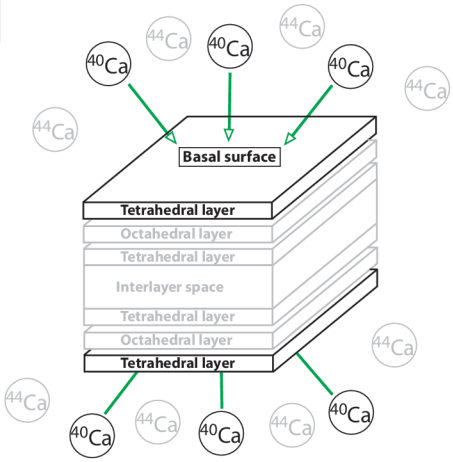

High selectivity for light isotopes (e.g., ^{40}**Ca**)

Heavy isotope (e.g., ^{44}**Ca**) **remain in solution**

Increase of solution $\delta^{44/40}$Ca signature

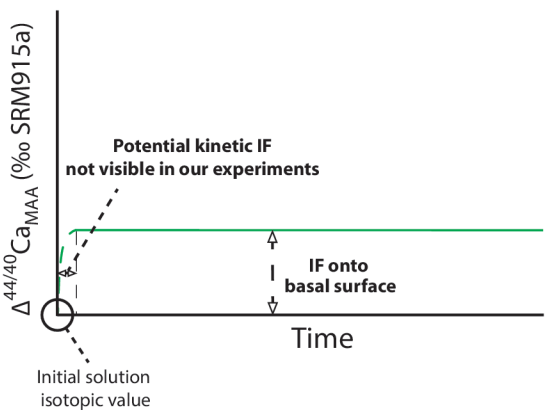

D

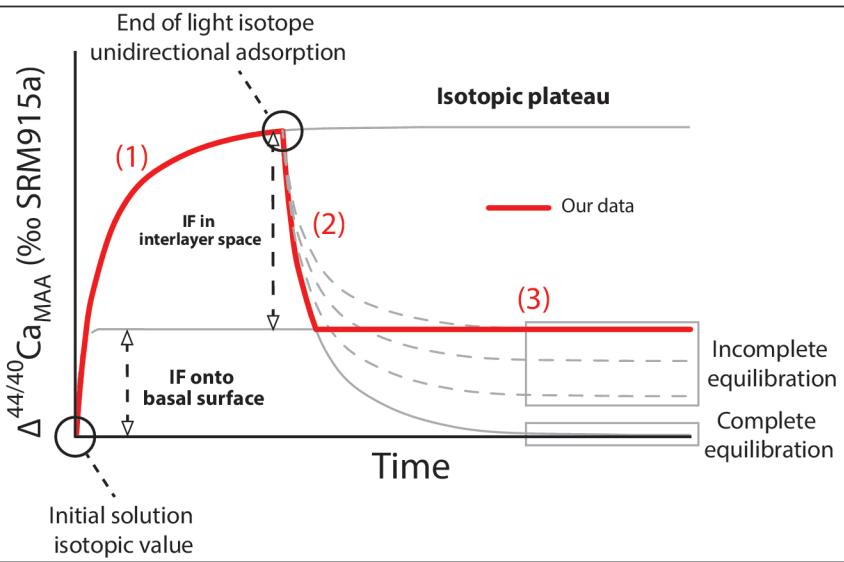

Results in this study

Initial Solution

KGa-2/Tuftane muscovite (50-200 μm)

Swy-2

Tuftane muscovite (0.1-1 μm)

0.0

-1.0

-2.0

-3.0

-4.0

-5.0

$\Delta^{44/40}Ca_{DES}$ (‰ SRM915a)

1.0

0.8

0.6

0.4

0.2

0.0

Fraction of Ca adsorbed onto the mineral

Phyllosilicate minerals	CEC méq.100g^{-1}	CEC represented by Na (%)	BET (N_2) Specific surface area ($m^2.g^{-1}$)	Layer charge	Interlayer space open to water and aqueous cations
KGa-2 (Kaolinite - 0.1-1 µm)	3.74	94.5	20.14	0/cell[1]	No[4]
Swy-2 (Montmorillonite – 0.1-1 µm)	74.6	90.1	28.60	0.6/cell[2]	Yes[4]
Tuftane muscovite (50-200 µm)	0.42	92.7	0.07	2/cell[3]	No[4]
Tuftane muscovite (0.1-1 µm)	46.7	94.2	62.23	2/cell[3]	No[4]

Sample	pH	$[Ca]_{IS}$ ($\mu mol.L^{-1}$)	Time (min)	Adsorbed Ca (μmol)	Adsorbed Ca (%)	$\Delta^{44/40}Ca_{MAA}$ 1 (‰ SRM915a)	$\Delta^{44/40}Ca_{MAA}$ 2 (‰ SRM915a)	$\Delta^{44/40}Ca_{MAAmean}$ (‰ SRM915a)	Uncertainties*
KGa-2	4	12.5	5	0.136	26	0.06	0.01	0.03	0.11
KGa-2	4	12.5	10	0.419	81	0.01		0.01	0.11
KGa-2	4	12.5	15	0.440	85	-0.08		-0.08	0.11
KGa-2	4	12.5	20	0.432	83				
KGa-2	4	12.5	35	0.413	80	0.07		0.07	0.11
KGa-2	4	12.5	65	0.327	63	0.06		0.06	0.11
KGa-2	4	12.5	125	0.264	51	-0.02		-0.02	0.18
KGa-2	4	12.5	425	0.216	42	-0.08		-0.08	0.11
KGa-2	4	12.5	1445	0.174	34	0.03		0.03	0.11
KGa-2	4	12.5	2885	0.153	29	-0.04		-0.04	0.13
KGa-2	7	29.9	5	0.541	45				
KGa-2	7	29.9	10	0.950	79	0.01		0.01	0.15
KGa-2	7	29.9	15	0.975	81				
KGa-2	7	29.9	20	0.963	80				
KGa-2	7	29.9	35	0.959	80	0.05		0.05	0.11
KGa-2	7	29.9	65	0.967	81	0.02		0.02	0.22
KGa-2	7	29.9	125	0.966	81				
KGa-2	7	29.9	425	0.957	80	0.07		0.07	0.12
KGa-2	7	29.9	1445	0.996	83	0.02		0.02	0.11
KGa-2	7	29.9	2885	0.960	80				
Swy-2	4	823	5	21.6	65	0.11		0.11	0.11
Swy-2	4	823	10	25.0	76	0.04	0.17	0.11	0.11
Swy-2	4	823	15	28.0	85	0.17		0.17	0.11
Swy-2	4	823	20	27.3	83	0.30	0.27	0.29	0.11
Swy-2	4	823	35	29.0	88	0.12	0.06	0.09	0.11
Swy-2	4	823	65	29.7	90	0.01		0.01	0.13
Swy-2	4	823	125	29.5	89	0.85		0.06	0.13
Swy-2	4	823	425	30.5	93	0.06		0.10	0.11
Swy-2	4	823	1445	29.8	91	0.17		0.17	0.11
Swy-2	4	823	2885	30.5	93	0.15		0.15	0.14
Swy-2	7	823	5	22.2	67	-0.04	0.06	0.02	0.11
Swy-2	7	823	10	29.3	89	0.16	0.17	0.16	0.11
Swy-2	7	823	15	28.9	88				
Swy-2	7	823	20	28.8	87	0.23	0.25	0.24	0.11
Swy-2	7	823	35	30.0	91	0.27	0.21	0.24	0.11
Swy-2	7	823	65	29.9	91	0.09	0.11	0.10	0.11
Swy-2	7	823	125	29.5	90	0.14	0.02	0.08	0.11
Swy-2	7	823	425	29.6	90	0.12		0.12	0.12
Swy-2	7	823	1445	28.7	87	0.12		0.12	0.11
Swy-2	7	823	2885	29.6	90	0.09		0.09	0.11
Tuftane muscovite (50-200 µm)	7	6.79	5	0.185	74	0.04		0.04	0.11

Tuftane muscovite (50-200 µm)	7	6.79	10	0.191	77	0.07	0.07	0.11
Tuftane muscovite (50-200 µm)	7	6.79	15	0.211	85			
Tuftane muscovite (50-200 µm)	7	6.79	20	0.211	85	0.04	0.04	0.11
Tuftane muscovite (50-200 µm)	7	6.79	35	0.210	84			
Tuftane muscovite (50-200 µm)	7	6.79	65	0.211	85			
Tuftane muscovite (50-200 µm)	7	6.79	125	0.211	85	0.07	0.07	0.11
Tuftane muscovite (50-200 µm)	7	6.79	425	0.207	83	-0.04	-0.04	0.11
Tuftane muscovite (50-200 µm)	7	6.79	1445	0.205	82	0.00	0.00	0.11
Tuftane muscovite (50-200 µm)	7	6.79	2885	0.205	82	-0.06	-0.06	0.13
Tuftane muscovite (0.1-1 µm)	4	182	5	1.41	19			
Tuftane muscovite (0.1-1 µm)	4	182	10	4.74	65	0.27	0.27	0.11
Tuftane muscovite (0.1-1 µm)	4	182	15	5.11	70			
Tuftane muscovite (0.1-1 µm)	4	182	20	4.90	67			
Tuftane muscovite (0.1-1 µm)	4	182	35	5.73	79	0.22	0.22	0.15
Tuftane muscovite (0.1-1 µm)	4	182	65	5.78	79			
Tuftane muscovite (0.1-1 µm)	4	182	125	5.79	79	0.22	0.22	0.12
Tuftane muscovite (0.1-1 µm)	4	182	425	5.76	79			
Tuftane muscovite (0.1-1 µm)	4	182	1445	5.83	80	0.24	0.24	0.11
Tuftane muscovite (0.1-1 µm)	4	182	2885	5.88	81			
Tuftane muscovite (0.1-1 µm)	7	182	5	3.30	45			
Tuftane muscovite (0.1-1 µm)	7	182	10	5.53	76	0.21	0.21	0.14
Tuftane muscovite (0.1-1 µm)	7	182	15	5.96	82			
Tuftane muscovite (0.1-1 µm)	7	182	20	6.17	85			
Tuftane muscovite (0.1-1 µm)	7	182	35	6.50	89	0.22	0.22	0.11
Tuftane muscovite (0.1-1 µm)	7	182	65	6.37	87			
Tuftane muscovite (0.1-1 µm)	7	182	125	6.42	88	0.23	0.23	0.11
Tuftane muscovite (0.1-1 µm)	7	182	425	6.55	90			
Tuftane muscovite (0.1-1 µm)	7	182	1445	6.54	90	0.24	0.24	0.11
Tuftane muscovite (0.1-1 µm)	7	182	2885	6.52	90			

Sample	pH	$[Ca]_{IS}$ ($\mu mol.L^{-1}$)	Time (min)	Desorbed Ca (MAD) (μmol)	[HC] ($mol.L^{-1}$)	Ca in HC solution (%)	Ca in residual liquid (%)	Corrected desorbed Ca (μmol)	Desorbed Ca (%)	$\Delta^{44/40}Ca_{MAD}$ 1 (‰ SRM915a)	$\Delta^{44/40}Ca_{MAD}$ 2 (‰ SRM915a)	$\Delta^{44/40}Ca_{MAD}$ mean (‰ SRM915a)	$\Delta^{44/40}Ca_{MAD}$ corrected (‰ SRM915a)	Uncertainties*
KGa-2	4	12.5	5	0.143	10^{-4}	0.12	6	0.135	99					
KGa-2	4	12.5	10	0.437	10^{-4}	0.04	2	0.428	102	-0.06		-0.06	-0.06	0.11
KGa-2	4	12.5	15	0.457	10^{-4}	0.04	2	0.448	102					
KGa-2	4	12.5	20	0.432	10^{-4}	0.04	2	0.423	98					
KGa-2	4	12.5	35	0.421	10^{-4}	0.04	2	0.413	100	0.04		0.04	0.04	0.11
KGa-2	4	12.5	65	0.339	10^{-4}	0.05	2	0.332	102					
KGa-2	4	12.5	125	0.274	10^{-4}	0.07	3	0.266	101	-0.03		-0.03	-0.03	0.11
KGa-2	4	12.5	425	0.227	10^{-4}	0.08	3	0.220	102					
KGa-2	4	12.5	1445	0.179	10^{-4}	0.10	4	0.172	99	0.02		0.02	0.03	0.11
KGa-2	4	12.5	2885	0.159	10^{-4}	0.11	5	0.151	99					
KGa-2	7	29.9	5		10^{-4}	0.03	2	0.534	99	-0.07		-0.07	-0.07	0.11
KGa-2	7	29.9	10	0.545	10^{-4}	0.02	1	0.949	100	-0.04		-0.04	-0.04	0.11
KGa-2	7	29.9	15	0.959	10^{-4}	0.02	1	1.001	103	0.01		0.01	0.01	0.11
KGa-2	7	29.9	20	1.01	10^{-4}	0.02	1	0.994	103	0.01	0.02	0.01	0.01	0.11
KGa-2	7	29.9	35	1.00	10^{-4}	0.02	1	0.988	103	0.02		0.02	0.02	0.11
KGa-2	7	29.9	65	0.998	10^{-4}	0.02	1	0.987	102	-0.02		-0.02	-0.02	0.11
KGa-2	7	29.9	125	0.997	10^{-4}	0.02	1	0.967	100	0.01		0.01	0.01	0.11
KGa-2	7	29.9	425	0.977	10^{-4}	0.02	1	0.981	103	0.01		0.01	0.01	0.11
KGa-2	7	29.9	1445	0.991	10^{-4}	0.02	1	0.977	98	0.01		0.01	0.01	0.11
KGa-2	7	29.9	2885	0.987	10^{-4}	0.02	1	0.954	99	0.00	0.09	0.05	0.05	0.11
Swy-2	4	823	5	22.9	10^{-2}	0.08	4	22.0	102					
Swy-2	4	823	10	26.5	10^{-2}	0.07	4	25.5	102					
Swy-2	4	823	15	29.5	10^{-2}	0.06	3	28.6	102					
Swy-2	4	823	20	28.6	10^{-2}	0.06	4	27.5	101	0.03			0.03	0.11
Swy-2	4	823	35	30.2	10^{-2}	0.06	2	29.6	102	0.07			0.07	0.11
Swy-2	4	823	65	31.0	10^{-2}	0.06	3	30.1	101					
Swy-2	4	823	125	30.5	10^{-2}	0.06	3	29.6	101	0.11			0.11	0.11
Swy-2	4	823	425	31.7	10^{-2}	0.06	4	30.5	100					
Swy-2	4	823	1445	31.0	10^{-2}	0.06	3	30.1	101					
Swy-2	4	823	2885	31.8	10^{-2}	0.06	4	30.6	100	0.03			0.03	0.11
Swy-2	7	823	5	23.6	10^{-2}	0.08	4	22.7	102					
Swy-2	7	823	10	31.5	10^{-2}	0.06	4	30.3	103					
Swy-2	7	823	15	29.5	10^{-2}	0.06	2	28.9	100					
Swy-2	7	823	20	30.1	10^{-2}	0.06	2	29.5	103	0.12			0.13	0.11
Swy-2	7	823	35	31.8	10^{-2}	0.06	3	30.9	103	0.08			0.08	0.11
Swy-2	7	823	65	31.2	10^{-2}	0.06	4	30.0	100					
Swy-2	7	823	125	30.8	10^{-2}	0.06	3	29.9	101	0.07			0.07	0.11
Swy-2	7	823	425	30.4	10^{-2}	0.06	3	29.5	100					
Swy-2	7	823	1445	30.4	10^{-2}	0.06	3	29.5	103					
Swy-2	7	823	2885	30.6	10^{-2}	0.06	3	29.5	100	-0.03			-0.03	0.12

Tuftane muscovite (50-200 µm)	7	6.79	5	0.192	10^{-4}	0.09	1	0.190	102	-0.05	-0.05	0.11
Tuftane muscovite (50-200 µm)	7	6.79	10	0.199	10^{-4}	0.09	1	0.197	103	0.07	0.08	0.11
Tuftane muscovite (50-200 µm)	7	6.79	15	0.210	10^{-4}	0.09	1	0.208	99			
Tuftane muscovite (50-200 µm)	7	6.79	20	0.212	10^{-4}	0.08	1	0.210	100			
Tuftane muscovite (50-200 µm)	7	6.79	35	0.208	10^{-4}	0.09	1	0.206	98	-0.03	-0.02	0.11
Tuftane muscovite (50-200 µm)	7	6.79	65	0.214	10^{-4}	0.08	1	0.212	100			
Tuftane muscovite (50-200 µm)	7	6.79	125	0.214	10^{-4}	0.08	1	0.212	100			
Tuftane muscovite (50-200 µm)	7	6.79	425	0.209	10^{-4}	0.09	1	0.207	100			
Tuftane muscovite (50-200 µm)	7	6.79	1445	0.204	10^{-4}	0.09	1	0.202	99	0.11	0.11	0.11
Tuftane muscovite (50-200 µm)	7	6.79	2885	0.211	10^{-4}	0.09	1	0.209	102	0.06	0.06	0.11
Tuftane muscovite (0.1-1 µm)	4	182	5	1.49	10^{-3}	0.11	3	1.44	103			
Tuftane muscovite (0.1-1 µm)	4	182	10	4.90	10^{-3}	0.04	1	4.85	102	-0.06	-0.06	0.12
Tuftane muscovite (0.1-1 µm)	4	182	15	5.22	10^{-3}	0.03	2	5.12	100			
Tuftane muscovite (0.1-1 µm)	4	182	20	5.05	10^{-3}	0.04	1	5.00	102			
Tuftane muscovite (0.1-1 µm)	4	182	35	5.77	10^{-3}	0.03	1	5.71	100	-0.02	-0.02	0.11
Tuftane muscovite (0.1-1 µm)	4	182	65	5.76	10^{-3}	0.03	1	5.70	99			
Tuftane muscovite (0.1-1 µm)	4	182	125	5.72	10^{-3}	0.03	1	5.66	98	0.03	0.03	0.12
Tuftane muscovite (0.1-1 µm)	4	182	425	5.83	10^{-3}	0.03	1	5.77	100			
Tuftane muscovite (0.1-1 µm)	4	182	1445	5.86	10^{-3}	0.03	1	5.80	100	0.01	0.01	0.11
Tuftane muscovite (0.1-1 µm)	4	182	2885	5.92	10^{-3}	0.03	1	5.86	100			
Tuftane muscovite (0.1-1 µm)	7	182	5	3.73	10^{-3}	0.05	1	3.69	112			
Tuftane muscovite (0.1-1 µm)	7	182	10	5.73	10^{-3}	0.03	1	5.67	102	-0.07	-0.07	0.11
Tuftane muscovite (0.1-1 µm)	7	182	15	6.16	10^{-3}	0.03	1	6.10	102			
Tuftane muscovite (0.1-1 µm)	7	182	20	6.26	10^{-3}	0.03	1	6.20	101			
Tuftane muscovite (0.1-1 µm)	7	182	35	6.57	10^{-3}	0.03	1	6.50	100	0.07	0.07	0.11
Tuftane muscovite (0.1-1 µm)	7	182	65	6.42	10^{-3}	0.03	1	6.35	100			
Tuftane muscovite (0.1-1 µm)	7	182	125	6.57	10^{-3}	0.03	1	6.50	101	-0.04	-0.04	0.11
Tuftane muscovite (0.1-1 µm)	7	182	425	6.72	10^{-3}	0.03	1	6.65	102			
Tuftane muscovite (0.1-1 µm)	7	182	1445	6.65	10^{-3}	0.03	1	6.58	101	0.00	0.00	0.11
Tuftane muscovite (0.1-1 µm)	7	182	2885	6.69	10^{-3}	0.03	1	6.62	101			

Sample	pH	Time (min)	$[Ca]_{IS}$ ($\mu mol.L^{-1}$)	$[K]_{IS}$ ($\mu mol.L^{-1}$)	$[Sr]_{IS}$ ($\mu mol.L^{-1}$)	$[Mg]_{IS}$ ($\mu mol.L^{-1}$)	$[Na]_{IS}$ ($\mu mol.L^{-1}$)	Adsorbed Ca (µmol)	Adsorbed Ca (%)	Adsorbed K (µmol)	Adsorbed K (%)	Adsorbed Sr (µmol)	Adsorbed Sr (%)	Adsorbed Mg (µmol)	Adsorbed Mg (%)	$\Delta^{44/40}Ca_{MAA}$ (‰ SRM915a)	Uncertainties*
Cationic competition																	
KGa-2 Test (1)	7	125	29.9	35.2	30.6	27.1	/	0.494	39	0.305	22	0.702	57	0.441	41	-0.05	0.11
KGa-2 Test (1/2)	7	125	29.9	17.5	14.9	13.2	/	0.609	53	0.155	22	0.353	59	0.278	53	0.07	0.12
KGa-2 Test (1/4)	7	125	29.9	8.64	7.25	6.49	/	0.765	70	0.073	22	0.211	73	0.170	65	0.03	0.11
Swy-2 Test (1)	7	125	823	1001	638	1014	/	14.5	45	10.9	27	16.3	64	19.1	47	-0.04	0.13
Swy-2 Test (1/2)	7	125	823	499	317	509	/	19.4	59	5.48	27	8.55	65	12.0	58	0.03	0.11
Swy-2 Test (1/4)	7	125	823	245	158	253	/	24.4	74	3.03	30	5.21	78	7.36	70	0.09	0.11
NaCl ionic strength																	
KGa-2 Test (10^{-1})	7	125	29.9	/	/	/	10^{5}	/	/	/	/	/	/	/	/	0.00	0.11
KGa-2 Test (10^{-2})	7	125	29.9	/	/	/	10^{4}	0.386	32	/	/	/	/	/	/	0.03	0.11
KGa-2 Test (10^{-3})	7	125	29.9	/	/	/	10^{3}	0.889	74	/	/	/	/	/	/	0.01	0.14
Swy-2 Test (10^{-1})	7	125	823	/	/	/	10^{5}	9.22	28	/	/	/	/	/	/	-0.05	0.12
Swy-2 Test (10^{-2})	7	125	823	/	/	/	10^{4}	12.1	37	/	/	/	/	/	/	0.02	0.12
Swy-2 Test (10^{-3})	7	125	823	/	/	/	10^{3}	24.5	74	/	/	/	/	/	/	0.09	0.13

Sample	pH	Time (min)	Desorbed Ca (µmol)	[HC] ($mol.L^{-1}$)	Ca in HC solution (%)	Ca in residual liquid (%)	Corrected desorbed Ca (µmol)	Desorbed Ca (%)	Desorbed K (µmol)	Desorbed K (%)	Desorbed Sr ($\mu mol.g^{-1}$)	Desorbed Sr (%)	Desorbed Mg (µmol)	Desorbed Mg (%)	$\Delta^{44/40}Ca_{MAD}$ (‰ SRM915a)	$\Delta^{44/40}Ca_{MAD}$ corrected (‰ SRM915a)	Uncertainties*
Cationic competition																	
KGa-2 Test (1)	7	125	0.516	10^{-4}	0.03	1	0.511	104	0.083	27	6.96	99	0.013	3	0.01	0.02	0.11
KGa-2 Test (1/2)	7	125	0.635	10^{-4}	0.03	1	0.629	103	0.053	34	3.51	99	0.009	3	-0.05	-0.05	0.14
KGa-2 Test (1/4)	7	125	0.780	10^{-4}	0.02	1	0.772	101	0.033	45	2.15	102	0.006	4	-0.07	-0.07	0.11
Swy-2 Test (1)	7	125	15.2	10^{-2}	0.11	6	14.3	98	3.10	29	159	97	0.554	3	0.08	0.09	0.11
Swy-2 Test (1/2)	7	125	19.6	10^{-2}	0.09	4	18.8	97	2.16	39	86.7	101	0.415	3	0.03	0.03	0.18
Swy-2 Test (1/4)	7	125	25.3	10^{-2}	0.07	3	24.5	100	1.52	50	51.7	99	0.293	4	0.12	0.12	0.11
NaCl ionic strength																	
KGa-2 Test (10^{-1})	7	125	0.020	10^{-4}	0.87	14	0.000	/	/	/	/	/	/	/	0.01	0.01	0.11
KGa-2 Test (10^{-2})	7	125	0.394	10^{-4}	0.04	1	0.390	101	/	/	/	/	/	/	0.10	0.10	0.12
KGa-2 Test (10^{-3})	7	125	0.908	10^{-4}	0.02	0	0.908	102	/	/	/	/	/	/	-0.02	-0.02	0.14
Swy-2 Test (10^{-1})	7	125	10.0	10^{-2}	0.17	7	9.36	102	/	/	/	/	/	/	0.04	0.04	0.11
Swy-2 Test (10^{-2})	7	125	13.3	10^{-2}	0.13	9	12.2	100	/	/	/	/	/	/	0.04	0.05	0.14
Swy-2 Test (10^{-3})	7	125	26.0	10^{-2}	0.07	4	25.0	102	/	/	/	/	/	/	-0.01	-0.01	0.11

Layer types	Groups	Layer charge (p.f.u.)	Interlayer space
1:1	Serpentine-kaolin	~0	No accessible
2:1	Talc-pyrophyllite	~0	No accessible
	Smectite	0.2-0.6	Open to hydrated cations adsorption
	Vermiculite	0.6-0.9	
	True mica	0.85-1.0	Closed by non-hydrated monovalent cations
	Interlayer-deficient mica	0.6-0.85	Closed by mono- or divalent non hydrated cations
	Brittle mica	1.8-2.0	Closed by divalent non-hydrated cations
	Chlorite	variable	Hydroxide sheet
2:1	Variable	variable	Regularly interstratified